

UC Davis

UC Davis Previously Published Works

Title

Assembly mechanism and cryoEM structure of RecA recombination nucleofilaments from *Streptococcus pneumoniae*

Permalink

<https://escholarship.org/uc/item/9x5331x5>

Journal

Nucleic Acids Research, 51(6)

ISSN

0305-1048

Authors

Hertzog, Maud
Perry, Thomas Noé
Dupaigne, Pauline
et al.

Publication Date

2023-04-11

DOI

10.1093/nar/gkad080

Peer reviewed

Assembly mechanism and cryoEM structure of RecA recombination nucleofilaments from *Streptococcus pneumoniae*

Maud Hertzog^{1,7,*}, Thomas Noé Perry^{2,†}, Pauline Dupaigne^{1b,3,†}, Sandra Serres¹, Violette Morales¹, Anne-Lise Soulet¹, Jason C. Bell⁴, Emmanuel Margeat⁵, Stephen C. Kowalczykowski^{1b,6}, Eric Le Cam³, Rémi Fronzes^{1b,2,*} and Patrice Polard^{1,*}

¹Laboratoire de Microbiologie et de Génétique Moléculaire (UMR 5100). Centre de Biologie Intégrative; 169, avenue Marianne Grunberg-Manago; CNRS - Université Paul Sabatier - Bât 4R4, 118, route de Narbonne; 31062 Toulouse cedex 09, France, ²Structure and Function of Bacterial Nanomachines – Institut Européen de Chimie et Biologie, Microbiologie fondamentale et pathogénicité, UMR 5234, CNRS, University of Bordeaux, 2 rue Robert Escarpit, 33600 Pessac, France, ³Genome Maintenance and Molecular Microscopy UMR 9019 CNRS, Université Paris-Saclay, Gustave Roussy, F-94805 Villejuif Cedex, France, ⁴10x Genomics, Inc., Pleasanton, CA, USA, ⁵CBS (Centre de Biologie Structurale), Univ Montpellier, CNRS, INSERM, Montpellier, France, ⁶Department of Microbiology and Molecular Genetics and Department of Molecular and Cellular Biology, University of California, Davis, CA 95616, USA and ⁷Present address: Unité de biologie Moléculaire, Cellulaire et du Développement (UMR 5077) Centre de Biologie Intégrative; 169, avenue Marianne Grunberg-Manago, CNRS - Université Paul Sabatier - Bât 4R4, 118, route de Narbonne 31062, Toulouse cedex 09, France

Received September 20, 2022; Revised January 19, 2023; Editorial Decision January 20, 2023; Accepted January 24, 2023

ABSTRACT

RecA-mediated homologous recombination (HR) is a key mechanism for genome maintenance and plasticity in bacteria. It proceeds through RecA assembly into a dynamic filament on ssDNA, the presynaptic filament, which mediates DNA homology search and ordered DNA strand exchange. Here, we combined structural, single molecule and biochemical approaches to characterize the ATP-dependent assembly mechanism of the presynaptic filament of RecA from *Streptococcus pneumoniae* (*SpRecA*), in comparison to the *Escherichia coli* RecA (*EcRecA*) paradigm. *EcRecA* polymerization on ssDNA is assisted by the Single-Stranded DNA Binding (SSB) protein, which unwinds ssDNA secondary structures that block *EcRecA* nucleofilament growth. We report by direct microscopic analysis of *SpRecA* filamentation on ssDNA that neither of the two paralogous pneumococcal SSBs could assist the extension of *SpRecA* nucleopolymers. Instead, we found that the conserved RadA helicase promotes *SpRecA* nucleofilamentation in an ATP-dependent manner. This al-

lowed us to solve the atomic structure of such a long native *SpRecA* nucleopolymer by cryoEM stabilized with ATP γ S. It was found to be equivalent to the crystal structure of the *EcRecA* filament with a marked difference in how RecA mediates nucleotide orientation in the stretched ssDNA. Then, our results show that *SpRecA* and *EcRecA* HR activities are different, in correlation with their distinct ATP-dependent ssDNA binding modes.

INTRODUCTION

Homologous recombination (HR) is a DNA strands exchange process essential for multiple pathways of genome maintenance and plasticity in all kingdoms of life (1,2). Defects in any of these pathways lead to deleterious consequences, such as cell death or various types of cancer (3). HR relies on the pairing of a single-stranded DNA (ssDNA) molecule with one complementary strand in a double-stranded DNA (dsDNA) to generate a three-stranded DNA structure, commonly referred to as a synaptic product or a D-loop structure (for displacement-loop) (4). This reaction is catalyzed by a widespread and conserved group of enzymes, defined hereafter as HR recombinases and named

*To whom correspondence should be addressed. Tel: +33 5 61 33 58 00; Email: maud.hertzog@univ-tlse3.fr
Correspondence may also be addressed to Rémi Fronzes. Tel: +33 5 40 00 25 61; Email: remi.fronzes@u-bordeaux.fr
Correspondence may also be addressed to Patrice Polard. Tel: +33 5 61 55 69 19; Email: patrice.polard@univ-tlse.fr

†The authors wish it to be known that, in their opinion, the first three authors should be regarded as Joint First Authors.

RecA in bacteria, Rad51/Dmcl in eukaryotes, RadA in archaea (distinct from the widespread bacterial RadA recombination effector (also referred to as SMS; (5)). They form the RecA/Rad51 protein family, unified by a conserved ATP binding and hydrolysis core domain and a common HR mechanism (2). They promote the pairing and exchange of homologous DNA molecules by polymerizing first on a ssDNA molecule to generate the so-called presynaptic nucleofilament (6). Once assembled, the presynaptic nucleofilament scans for an homologous sequence in dsDNA and promotes ssDNA pairing with a complementary DNA sequence to generate the D-loop (7). The assembly and disassembly of RecA/Rad51 nucleofilaments is finely tuned by the binding and hydrolysis of nucleotides at the interface between monomers in the polymer. As such, RecA/Rad51 nucleofilaments are dynamic and the regulation of the DNA-dependent NTP binding and hydrolysis cycle is at the heart of the HR process.

RecA from *Escherichia coli* (*EcRecA*) is a model protein for the bacterial HR recombinases (8). Crystal structures of a chimera made of 6 or 5 fused protomers of *EcRecA* truncated for N-terminal (1–30) and C-terminal (336–353) residues and bound to DNA in the presence of a non-hydrolyzable ATP derivative have revealed many key features about the organization of presynaptic filament assembly and the mechanism of its pairing with a complementary ssDNA molecule (9). First, ssDNA and ATP bind to RecA–RecA interfaces cooperatively, explaining the ATP dependency for RecA polymerization on ssDNA. Second, the γ -phosphate of ATP is sensed across the RecA–RecA interface by two lysine residues that stimulate ATP hydrolysis, providing a mechanism for DNA release. Third, the nucleoprotein filament adopts a right-handed helical shape with six *EcRecA* monomers per turn, which stretch the ssDNA about 1.6-fold in comparison with a B-form dsDNA. Remarkably, the ssDNA is organized in the filament in regularly separated B-form triplets of nucleotides, including two bases exposed externally that restricts the homology search to Watson–Crick-type base pairing within a recipient DNA. In addition, using a chimera of 9 fused *EcRecA* subunits, Yang et al. recently solved by high-resolution cryoEM the structure of a D-loop assembled by this chimeric *EcRecA* polymer in the presence of a non-hydrolyzable ATP derivative (10). In parallel to these advances in the structural organization of *EcRecA* nucleofilaments HR intermediates, intensive biochemical ‘ensemble’ studies along with the development of single molecule (SM) techniques using fluorescently labelled *EcRecA* revealed important aspects in the dynamics of its ATP-dependent polymerization on DNA at the pre-synaptic and synaptic HR steps (2,10–13). These studies highlighted a biased growth of *EcRecA* filaments along ssDNA from 5’ to 3’ direction in presence of ATP, and a bidirectional growth in presence of the poorly hydrolyzable ATP γ S analogue that stabilizes the *EcRecA* polymer on DNA. In addition, SM analysis provided a direct imaging of the slow initial *EcRecA* interaction on ssDNA prior to the rapid growth of the nucleofilament, referred to as the nucleation and extension stages, respectively (14). These SM studies also unveiled key features of the DNA homology search and subsequent pairing stages mediated by *EcRecA* presynaptic filament, which proceeds

through an inchworm mechanism and a 3-nucleotide stepping during DNA strand exchange, respectively (9). Similar structural and SM analysis conducted on Rad51/DMC1 pointed at the conservation of *EcRecA* properties in eukaryotic HR recombinases, pointing at their general character of these properties to all members of the RecA/Rad51 family (15).

Another common feature of HR recombinases is the assistance of accessory factors that modulate their polymerization/depolymerization from DNA templates and/or their DNA strands exchange activities (16). These HR modulators are differentially conserved, with some being found in a whole kingdom of life and others limited to few species. They compose distinct and partially overlapping subsets of HR effectors that define specific pathways of genome maintenance and plasticity. In bacteria, a widely conserved HR effector is the SSB protein (Single-Stranded DNA Binding). SSB is firstly known as being essential to cell growth *via* its action at the replication forks where it protects ssDNA and assists its replication by melting out secondary structures that could form of ssDNA and impede the progression of DNA polymerases. Reconstitution of *E. coli* HR *in vitro* has highlighted three distinct roles of its cognate SSB in counteracting or assisting its DNA interacting activities (17): one is to prevent RecA nucleation if bound first on the ssDNA; a second is to promote RecA polymerization along ssDNA, by removing the secondary structures that impede filament growth (providing the same assistance as to DNA polymerases); a third is to bind to the extruded parental strand during the DNA strand exchange reaction, stabilizing the recombination product and favoring the incorporation of ssDNA (a step referred to as a DNA branch migration). Another key and conserved bacterial effector acting in these postsynaptic stages of HR is RadA, which has been found to facilitate ssDNA recombination from D-loop structures *via* interaction with RecA and by driving DNA branch migration (5,18,19). Other known HR effectors act at one or more of these steps of the HR recombinase activity cycle through static or dynamic protein-protein interactions and/or DNA remodeling activities (3).

Not all bacterial RecAs exhibit the same intrinsic activities as *EcRecA*. Notable examples are RecA from *Deinococcus radiodurans* (*Dr*) and from *Pseudomonas aeruginosa* (*Pa*). These two bacterial species undergo high HR rate in their natural environment to sustain their growth under extreme radiative or oxidative conditions, respectively (20,21). *DrRecA* is less homologous to *EcRecA* than *PaRecA*, i.e. 61% and 71% of sequence identity, respectively. Their DNA binding affinity was found higher than that of *EcRecA*, along with a stronger ability to displace its cognate SSB from ssDNA for *PaRecA* and with a reverse recombination from dsDNA to ssDNA for *DrRecA*. Another reported deviation to the *EcRecA* paradigm is RecA from *Streptococcus pneumoniae* (*Sp*, the pneumococcus), which is well known to undergo high HR rate during the process of genetic transformation induced in response to multiple stress during the state of competence (22). Previous biochemical studies comparing *SpRecA* and *EcRecA* activities highlighted two marked differences between those two HR recombinases, which share 63% of identity. First, *SpRecA* was found intrinsically less efficient than *EcRecA* in directing

DNA strand exchange between a long circular ssDNA with a complementary strand in a linear duplex DNA (23) a feature shared by RecA from *Bacillus subtilis* (*BsRecA*)(24); second, *SpRecA* interaction with ssDNA appears to be negatively challenged in the presynaptic stages of HR and positively assisted during synapsis by any of its two cognate paralogous SSB proteins, namely SsbA and SsbB (the former being essential and involved in DNA replication and genome maintenance processes and the latter being restrictively expressed during competence and involved in the mechanism of natural transformation; (24,25)); of note, the lack of assistance by SsbA from *B. subtilis* to its cognate *BsRecA* in presynaptic stages has also been reported, while the second SsbB also encoded by *B. subtilis* and specifically induced during competence assists *BsRecA* polymerization on ssDNA in early HR steps. Altogether, what precisely determine these functional deviations of *SpRecA* and *BsRecA* in comparison with *EcRecA* remains enigmatic.

Here, we combined classical biochemical techniques with single-molecule and structural approaches to closely examine the DNA interacting properties of *SpRecA* in comparison with *EcRecA*. Together, these experiments highlight significant variations in the ATP-dependent dynamics and structure of the *SpRecA* presynaptic filament, including the lack of assistance in its elongation by any SSB protein. Unexpectedly, however, we found that the *SpRadA* helicase could promote such an extension of the *SpRecA* presynaptic filament in an ATP-dependent manner. Altogether, this detailed analysis provides important molecular insights into the distinct efficiency of *SpRecA* in catalyzing HR in comparison with *EcRecA*.

MATERIAL AND METHODS

Proteins

SpRecA, SsbA, SsbB and *E. coli* SSB proteins and derivatives were purified following the same procedure described previously (19). Briefly, RecA or Ssb proteins were purified as soluble and native proteins, without any tag, as recombinant species following classical overexpressed in *E. coli* from pT7-directed plasmids. Protein expression was induced by adding 0.5 mM IPTG (37 °C for 2 h) to exponentially grown cells. Cells were resuspended in sucrose buffer (25 mM Tris–Cl, pH 8, 25% sucrose, 1 mM EDTA, 200 $\mu\text{g ml}^{-1}$ lysozyme) before liquid nitrogen freezing. Cell pellets were next thawed overnight on ice and suspensions were clarified by ultracentrifugation. The clarified supernatant was transiently precipitated by addition of 0.1% Polymix P. After several salt washes, the protein fractions containing RecA or Ssb proteins were resolubilized in 20 mM Tris–Cl pH 7.6, 1 M NaCl, 1 mM DTT. The protein solution was then precipitated by ammonium sulfate. After centrifugation, the supernatants containing RecA and Ssb proteins were consecutively loaded on Phenyl, Heparin and Q columns and purified by FPLC.

EcRecA was purified following the same procedure as for *SpRecA*. Its ATPase and DNA strand exchange activities were found to be identical to those of commercial *EcRecA* from NEB. Thus, we used for this study either commercial or purified *EcRecA*.

D-loop assay

The basic reaction solution contained 10 mM Tris–Cl (pH 7.5), 0.1 mg/ml BSA, 8% glycerol, 0.5 mM DTT or TCEP, 50 mM NaCl, 10 mM MgAc, 2 mM ATP, 10 nM of 5' Cy3 100-mer oligonucleotide (5'-TGCTTCCGGCTCGTATGTTGTGTGGAATTGTGAGCGGATAACAATTTCACACAGGAAACAGCTATGACCATGATTACGAATTCGAGCTCGGTACCCGGGG-3') homologous to pUC18 sequence, and RecA (150–600 nM). After incubation of RecA with the ssDNA (oligonucleotide) for 10 min at 37 °C, we added 5 nM of pUC18 vector into the reaction and further incubated 10 min at 37 °C to allow oligonucleotide-pUC18 pairing (D-loop). The reaction was then kept on ice. The reaction was quenched (or deproteinized) with 1% SDS/10 mM EDTA (final concentrations). 0.5 μl of loading buffer (xylene cyanol in 30% glycerol) was added and reactions analysed by electrophoresis on a 1.2% agarose gel in a Tris-acetate–EDTA buffer at room temperature, 6 V/cm for 1 h in order to identify and estimate properly the amount of D-loop created. We detected the free and the bound Cy3 labelled oligonucleotides by a Fluor imager (Typhoon trio-Fuji-GE-healthcare) with an Abs/Em of 532/580 nm. Quantification of the proportion of D-loop created in this assay was performed with the Multigauge and Excel softwares.

TEM analysis

For transmission electron microscopy studies, a fraction of the reactions containing DNA-protein complexes was diluted and handled as previously described (26). For the reaction of RecA filament formation, 15 μM (nucleotides) ΦX ssDNA were first incubated with 5 μM *SpRecA* or *EcRecA* 15 min at 37 °C in a buffer containing 10 mM Tris–HCl pH 7.5, 50 mM KCl, 5 mM MgCl₂, 1 mM DTT and either 1.5 mM ATP or 1 mM ATP γ S or 1.5 mM ATP plus 1.5 mM BeF₃. In the experiments to test the assistance of RecA filament formation by SSB proteins, 0.25 μM (non-saturating amount) of either *EcSSB* or streptococcal SsbA or SsbB were added to the filament formation reaction 5 min after RecA. In some cases, saturating amount of *EcSSB* or SsbA or SsbB (1 μM) was added in the reaction. For statistical analysis of the length of filaments, 30–50 molecules were analyzed for each reaction.

Fluorescence labeling

SpRecA^{A488} was made by covalently modifying primary amines (lysines or N-ter) of the protein with Alexa 488-succinidimyl ester (Molecular Probes, ThermoFisher), in presence of an excess of ssDNA (M13 mp18, NEB) and ATP γ S (Roche) in order to preserve both ATP and ssDNA binding surfaces of the purified recombinant protein. The free fluorescent probe was removed by a step of gel filtration chromatography (Superdex 200 Increase 10/300 GL; GE Healthcare) in the reaction buffer 50 mM Tris (pH 7.5), 300 mM NaCl, 1 mM DTT. To remove any ATP or DNA contaminant, a final step of Anion Exchange chromatography was performed (MonoQ column GE Healthcare).

RecA^f was prepared as previously described (20). The ssDNA binding activity of RecA was determined by monitoring the ATP hydrolysis rate of RecA at increasing concentrations of ATP.

Production of DNA substrates

Gapped DNA substrates were prepared as described previously (27). The short fluorescent ssDNA substrate used in FCS experiments was prepared with synthetic oligonucleotides (Eurogentec) labeled either with Biotin or Alexa-488 in 5' in order to generate a Biotin-labeled DNA strand and a fluorescently-labeled DNA strand (Sequence : Biotin-5'GCTTGCATGCCTGCAGGTCG3'; Alexa488-5'GCGATAACAATTCACACAGG3') by PCR-amplification using the pUC18 plasmid as template. After PCR amplification (volume = 2 ml), the PCR reactions were loaded on Hi-Trap Streptavidin column (GE Healthcare). By addition of 60 mM NaOH, the fluorescent DNA strand is eluted, while the Biotin DNA strand remains on the column. The fluorescent ssDNA is then precipitated by Chloroform/Isopropyl alcohol, resuspended in 10 mM Tris-HCl pH 7.5; 50 mM NaCl and quantified using a Nanodrop spectrophotometer.

Direct imaging of RecA assembly on single molecules of ssDNA

A gapped ssDNA substrate was prepared and biotinylated as described in (27). The gapped ssDNA molecules were injected into a flow cell and tethered to the surface of a coverslip via biotin-streptavidin interactions. Flow cells (4 mm × 0.4 mm × 0.07 mm) were assembled using a glass slide, a coverslip, and double-sided tape (3M Adhesive Transfer Tape 9437). Ports were drilled into the glass microscope slide, and flow was controlled using a motor-driven syringe pump (28,29). The surface of the coverslip was cleaned by the subsequent injection of 1 M NaOH for 10 min, rinsed with water and equilibrated in buffer containing 20 mM TrisOAc (pH 8.0), 20% sucrose and 50 mM DTT. The surface was then functionalized by injecting the above buffer containing 2 mg/ml biotin-BSA (Pierce) and incubated for 10 min, rinsed with buffer, equilibrated with 0.2 mg/ml streptavidin (Promega) for 10 min and then blocked with 1.5 mg/ml Roche Blocking Reagent (Roche) for 10 min. For imaging, the gapped DNA were allowed to incubate in the flow cell in the absence of flow for ~5–15 min.

FCS measurements

Fluorescence correlation spectroscopy was performed on a custom-built setup with Pulse Interleaved Excitation (PIE) and Time Correlated Single Photon Counting (TCSPC) detection as described elsewhere (30). The FCS measurements were performed in the presence of the indicated amount of RecA proteins, 5 nM fluorescently labeled ssDNA (fluorescent probe: Alexa-488; size: 100 bases), in a buffer containing 10 mM Tris-HCl, pH 7.5; BSA 0.5 mg/ml; 4 mM MgCl₂; 50 mM NaCl; 0.5 mM DTT.

Equilibrium anisotropy fluorescent binding assays

Titration to monitor the binding of RecA to ssDNA were performed by monitoring the anisotropy of fluorescence enhancement at 25°C, using a Horiba fluorescence spectrophotometer set at an excitation wavelength of 495 nm and an emission wavelength of 520 nm. Excitation and emission slits were set to a bandwidth of 10 nm. Titrations were performed in 25 mM Tris-HCl (pH 7.5), 1 mM DTT, 25 mM NaCl, 2.5% glycerol, 10 mM MgCl₂ and the indicated concentration of nucleotide. The anisotropy of fluorescence values were corrected for dilution. An increased amount of RecA was added to the reaction solution containing the 25 nM of polydT of 65-mers. Data fitting using One-site-specific binding model was performed using GraphPad Prism. All equilibrium titrations were performed 3 times and the curves shown are the average of three with SEM represented.

Presynaptic and postsynaptic complex assembling

All the reaction steps were carried out at 37°C. For assembling presynaptic filaments, ΦX174 Virion single strand DNA (New England BioLabs) at 10 ATPγS g ml⁻¹ was incubated with RadA at 50 μg ml⁻¹ for 1 min in the reaction buffer comprising of 10 mM HEPES pH 7.5, 100 mM NaCl, 50 mM KCl, 0.5 mM DTT and 1.5 mM ATPγS; 50 μM Mg Cl₂. Then, SpRecA was added at final concentration of 200 μg ml⁻¹ for 3.5 h at 37°C. For assembling postsynaptic filaments, Lambda double strand DNA (New England BioLabs) at 10 μg ml⁻¹ was incubated with SpRecA at 200 μg ml⁻¹ for 3.5 h at 37°C in the same reaction buffer. Complex formation was checked by negative stain on a CM120 electron microscope (FEI/Thermo Fisher).

Cryo-EM specimen preparation and electron microscopy data acquisition

For cryo-EM analyses, 3.5 μl of sample were deposited on glow-discharged Lacey carbon grids, blotted with filter paper to remove excess sample for 4 s, and plunge-frozen in liquid ethane using a FEI Vitrobot Mark IV (FEI/Thermo Fisher) with a blotting force of 0 in an environment with 100% humidity and 4°C temperature. Cryo-EM images were acquired on a Falcon 3 direct detector in counting mode for the presynaptic complex and in linear mode for the postsynaptic complex on a FEI Talos Arctica at 200 kV. For the presynaptic complex, a magnification of 190 000× was applied to record 40 movie frames with an exposure time of 0.8 s using a dose rate of 0.9 electrons per Å² per frame for a total accumulated dose of 36 electrons per Å² at a pixel size of 0.76 Å. For the postsynaptic complex, a magnification of 120,000× was applied to record 20 movie frames with an exposure time of 1 s using a dose rate of 3 electrons per Å² per frame, resulting in a total accumulated dose of 60 electrons per Å² at a pixel size of 1.24 Å. The final datasets were composed of 2896 (for the presynaptic complex) and 2364 (for the postsynaptic complex) micrographs with defocus values ranging from -0.8 to -2.5 μm.

Helical reconstruction

Similar procedures were applied to the presynaptic complex and the postsynaptic complex datasets using helical reconstruction methods in RELION 2.1 (31). All frames were corrected for gain reference, binned by a factor of 2 only for the presynaptic complex, motion-corrected and dose-weighted using MOTIONCOR2 (32). Contrast transfer function (CTF) parameters were estimated by CTFind-4.1 (33).

Particles on micrographs of the presynaptic complex were picked manually in box sizes of 180 pixels and with an inter-box distance of 100 Å. Then, picked particles were classified into two-dimensional class averages to identify homogeneous subsets using a regularization value of $T = 2$. Selected classes were used as references for autopicking in RELION 2.1 (31). The total number of initial extracted segments (25653) was reduced to 7254 by subsequent rounds of two-dimensional classifications. After the best two-dimensional classes were selected, a first 3D reconstruction was done using featureless cylinder of 125 Å in diameter as an initial model. This was achieved by refining without imposing any helical symmetry and. This yielded a map at 7.6 Å in which helical symmetry was already apparent. The processing workflow is described in supplemental Figure 3.

Then, this map was used as reference for new autopicking on the micrographs of both complexes. The total number of extracted particles (363 828 segments for the presynaptic and 1 109 194 segments for the postsynaptic) was reduced to 188 475 and 715 954 by subsequent rounds of two-dimensional classifications. High-resolution refinements were performed in RELION's 3D auto-refinement using the non-symmetrized map as a reference, optimizing both the helical twist (58.46° and 58.62° respectively) and rise (15.38 and 14.97 Å, respectively). The final resolution was 3.9 Å for the presynaptic complex and 3.8 Å for the postsynaptic complex, calculated with two masked half-maps refined independently, according to the gold standard Fourier shell correlation (FSC) 0.143 criterion using RELION. Local resolution, calculated with RELION with a B -factor applied of -141.9 and -153.07 respectively, retrieved a range between 3.7 and 7.7 Å. All of the densities obtained were subjected to Auto-sharpening in the Phenix software package (34).

Model building and refinement

The initial atomic model of *SpRecA* protomers in both presynaptic and post-synaptic complexes were generated from the crystal structure of *E. coli* RecA (PDB ID: 3cmw and 3cmx) by SWISS-MODEL (35). Rigid-bodies, comprising four molecules of ATP γ S and the DNA, were docked into the auto-sharpened electron density map in UCSF-Chimera (36). The coordinates of the obtained single-chain model were modified manually using Coot and refined with repeated rounds of Phenix real-space refine function. The structure was further refined in real-space in PHENIX with secondary structure restraint (34). The atomic models were validated using the Cryo-EM validation tools of Phenix (37). Briefly, each model was firstly refined against the sharpened map (Supplemental data). To

monitor the refinement of the model and avoid over-fitting, the final model was refined against one half map and tested against the other half map by calculating the Fourier Shell Correlation curves (not reported), which indicated that the refinement of the atomic coordinates did not suffer from over-fitting. The asymmetric unit is composed of three protomers. We included four protomers to show the contacts between two adjacent asymmetric units. Extending the PDB further can just be obtained by applying the symmetry operators.

RESULTS

SpRecA forms short presynaptic filaments

First, we purified *SpRecA* and analyzed by transmission electron microscopy (TEM) its ATP-dependent polymerizing activity on ssDNA in comparison with purified *EcRecA*, by using circular form of Φ X174 bacteriophage (5386 nucleotides long) as a template. *SpRecA* added in saturating concentration to fully cover all ssDNA molecules forms dense structures on ssDNA in the presence of ATP (Figure 1B). These structures result from *SpRecA* binding to ssDNA as they are not observed with naked ssDNA (Figure 1A). The same experiment performed with an ATP regenerating system did not change the result (Figure 1C). By contrast, short polymers could be detected in the presence of the poorly hydrolysable ATP γ S derivative (Figure 1D). We also observed similar extended filaments in the presence of ATP and of BeF₃, a Pi analogue known to notably inhibit ATP hydrolysis (Figure 1E and Supplemental Figure 1). The same TEM analysis performed with *EcRecA* showed that it also forms small dense structures on ssDNA (Figure 1F) in the presence of ATP. By contrast, *EcRecA* was able to form extended filaments in the presence of ATP together with an ATP regenerating system (Figure 1G), showing not only its binding but also its assembly along ssDNA. Furthermore, *EcRecA* appeared to polymerize extensively along Φ X174 ssDNA in the presence of ATP γ S (Figure 1H), and for a 6-fold longer distance than *SpRecA* in the same conditions (mean value of 767 and 122 nm, respectively; see Figure 1I). Both recombinases could generate several filaments on the same Φ X174 ssDNA molecule in experiments performed with ATP γ S, indicative of several nucleation events for both recombinases followed by their polymerization. The total length of *SpRecA* nucleofilaments per individual ssDNA molecule was ~ 0.34 μ m in the presence of ATP γ S (and ~ 0.47 μ m in the presence of ATP and BeF₃), contrasting with the ~ 2.06 μ m measured for *EcRecA* in the presence of ATP γ S. Also, in these conditions, *EcRecA* does not fully cover the circular ssDNA template, indicating that its polymerization is blocked at some sites, most probably secondary structures that formed on ssDNA (27). Interestingly, *SpRecA* seems to be less efficient than *EcRecA* to unfold such structures, explaining why *SpRecA* generate more and shorter filaments on the long ssDNA template. Altogether, these results revealed a marked difference between *SpRecA* and *EcRecA* in their ability to extend their nucleofilamentation under these stabilizing conditions that block ATP hydrolysis and their release from ssDNA.

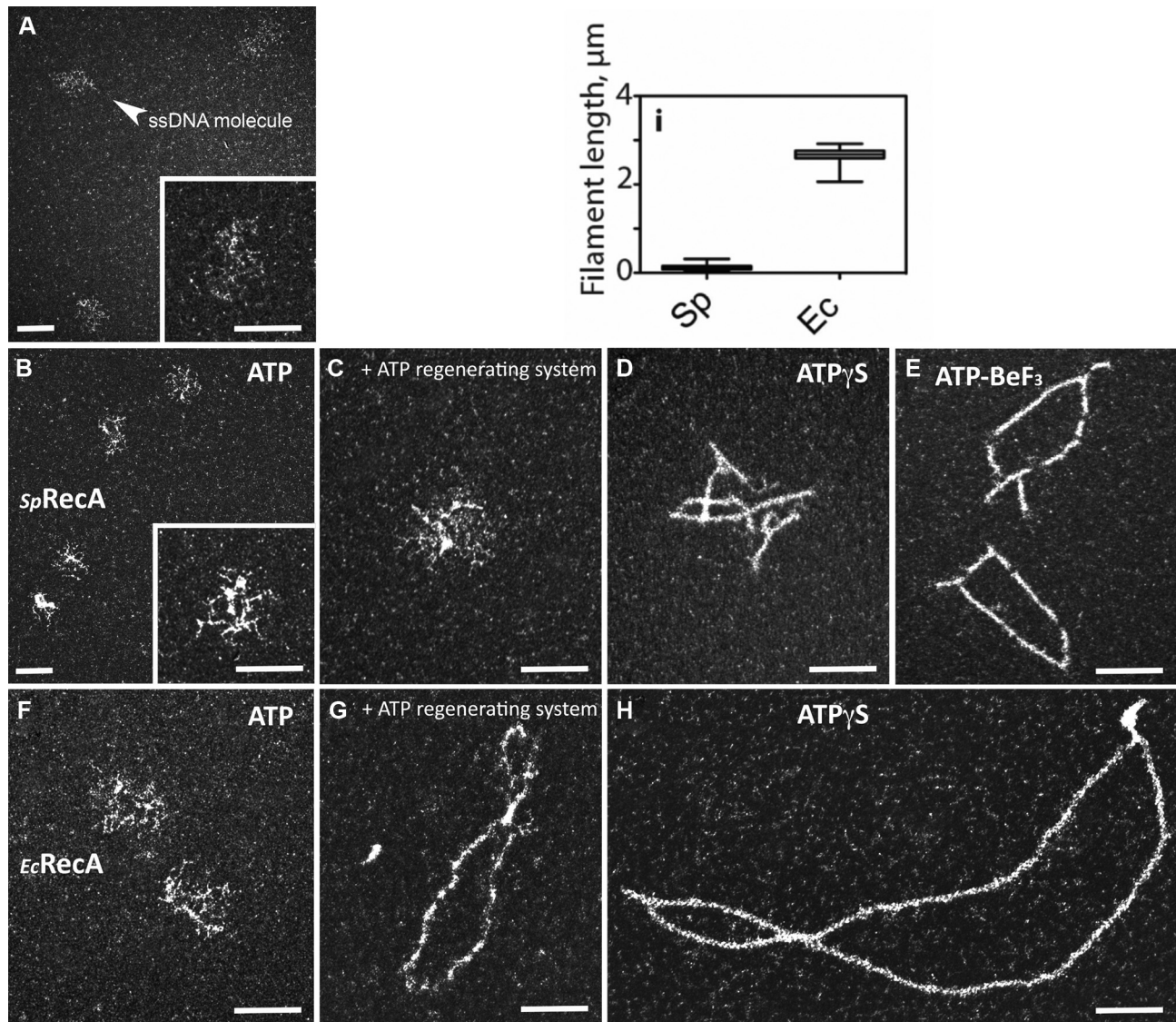


Figure 1. TEM analysis of *SpRecA* and *EcRecA* polymerisation on ssDNA. From a to h, representative electron micrographs images of ΦX ssDNA alone (A) or incubated with *SpRecA* and ATP (B), *SpRecA*, ATP and an ATP regenerating system (C), *SpRecA* and $ATP\gamma S$ (D), *SpRecA* and $ATP-BeF_3$ (E), with *EcRecA* and ATP (F), *RecA_{Ec}*, ATP and an ATP regenerating system (G), *RecA_{Ec}* and $ATP\gamma S$ (H). In (I): measured length of the filaments made with *EcRecA* or *SpRecA* in presence of $ATP\gamma S$ (50 molecules per experiments, $n = 2$). All scale bars represent 200 nm.

***SpRecA* polymerisation on ssDNA is not assisted by any SSB protein.**

EcRecA presynaptic filamentation is well known to be assisted by its cognate SSB *via* its melting activity of secondary structures that form on ssDNA (38). This has been generalized to several bacterial RecA similarly studied *in vitro*, with the marked exceptions of *SpRecA* and *BsRecA* (17). Indeed, *E. coli* SSB appears to counteract the presynaptic HR step of *SpRecA*, as indirectly evaluated by measuring the rate of ssDNA induced *SpRecA* ATP hydrolysis, while still stimulating the subsequent DNA strand exchange step (25). This negative competitive effect of SSB on *SpRecA* interaction with ssDNA evaluated in similar ATPase assays was observed with any of the two paralogous pneumococcal SSB, SsbA and SsbB (39,40). Conversely, SsbA and SsbB behave similarly as *EcSSB* in stimulating *EcRecA* ATPase

and HR activities. These earlier studies pointed at a distinct HR activity of *SpRecA* in comparison with *EcRecA*, which is differently challenged by SSB proteins. We studied by TEM this interplay between *SpRecA* and SSB proteins. Typical images obtained by TEM using saturating amounts of SsbA and SsbB (1 μM) incubated with $\Phi X174$ ssDNA template are presented in Figure 2A and B, respectively, revealing an identical pattern of interaction with ssDNA. Based on what is commonly done to achieve *EcRecA* filament formation *in vitro*, a non-saturating concentration of SsbA/SsbB (0.25 μM) was added to *SpRecA* pre-bound to ssDNA to test their potential ability to assist *SpRecA* filament elongation. Addition of either of these two SSB proteins in the reaction in the presence of ATP alone or with an ATP regenerating system did not promote *SpRecA* polymerization but rather led to the same nucleocomplexes

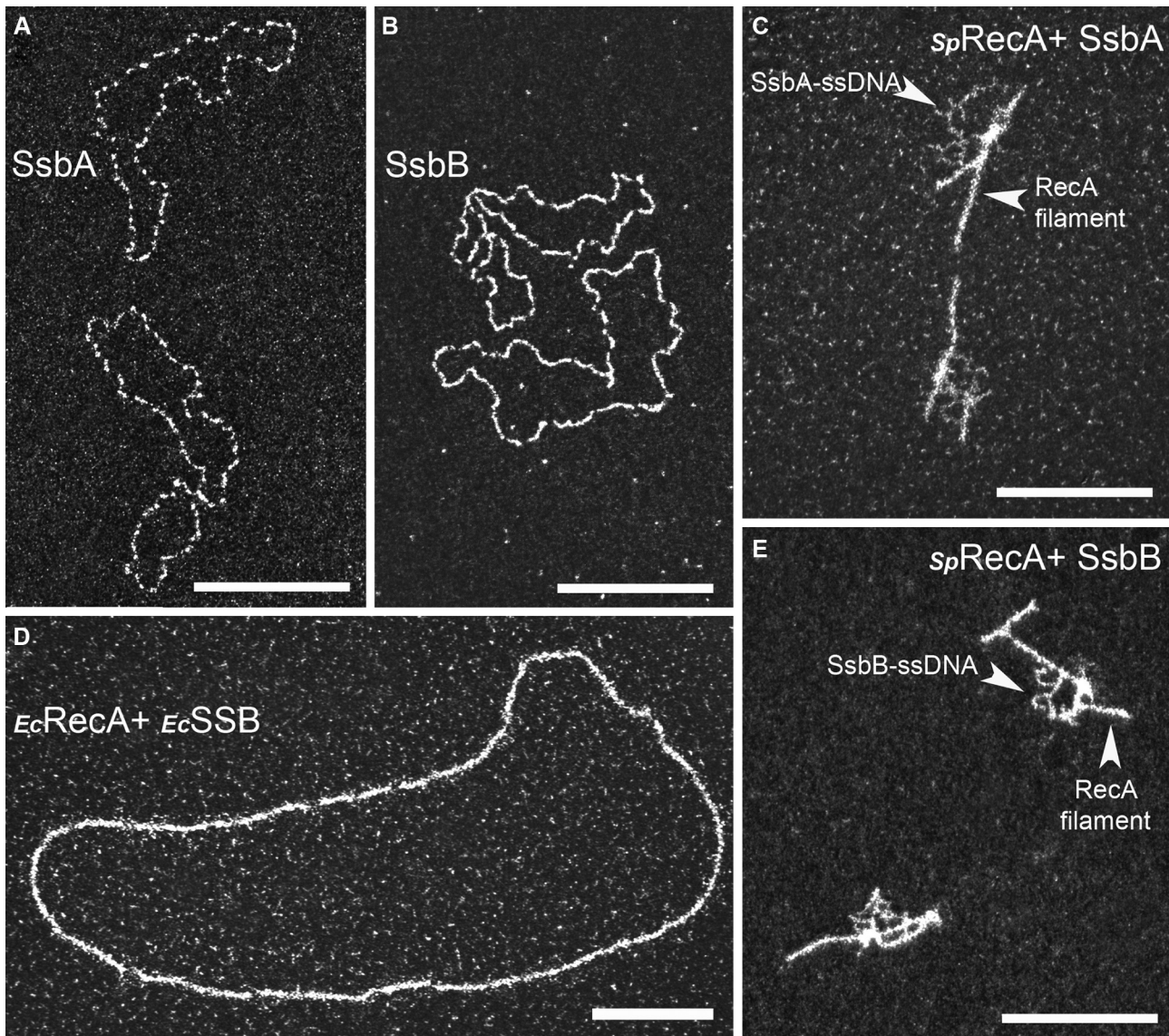


Figure 2. TEM analysis of *SpRecA* and *EcRecA* assembly on ssDNA in presence of *SpSsbA* and *SpSsbB*, or *EcSSB*. Representative electron micrographs images of ΦX ssDNA (15 μM) incubated either with saturating amount (1 μM) of SsbA (A) or SsbB (B), or pre-incubated with *SpRecA* and, next, incubated with non-saturating amount (0,25 μM) of SsbA (C) or SsbB (E), or pre-incubated with *EcRecA* and, next, incubated with non-saturating amount of *EcSSB* (D). All scale bars represent 200 nm.

observed with the SSBs alone. In the same vein, addition of SsbA or SsbB to the short *SpRecA* filaments formed in the presence of ATP γ S did not promote their elongation but led to the binding of either of these two SSBs to the ssDNA unoccupied by *SpRecA* (Figures 2C and E, respectively). By contrast, we confirmed that *EcSSB* added to *EcRecA* pre-incubated with ssDNA in the presence of ATP γ S promotes a full coverage of the circular ssDNA molecules by *EcRecA* (Figure 2D). The same result has been obtained by adding *EcSSB* to *EcRecA* incubated with ssDNA in the presence of ATP and an ATP regenerating system. Furthermore, we also found that *EcRecA* polymerization along ssDNA could also be assisted by the two pneumococcal SSBs and, conversely, that *EcSSB* failed to assist *SpRecA* nucleofilamentation in any conditions. Altogether, these findings highlight that *SpRecA* ATP-dependent fila-

mentation on ssDNA is not assisted by any SSB, highlighting a main functional deviation between *SpRecA* and the *EcRecA* paradigm and all other RecA proteins similarly studied so far.

The *SpRadA* HR helicase extends *SpRecA* polymerization on ssDNA.

We next wondered whether *SpRecA* nucleofilamentation on ssDNA could be assisted by another HR effector. An obvious candidate was the *SpRadA* protein, which we found to interact with RecA and to be a DnaB-type hexameric helicase that canonically translocates along ssDNA fueled by ATP hydrolysis in the 5' to 3' direction (19). We investigated by TEM analysis whether *SpRadA* could modulate *SpRecA* extension along ssDNA, by using the circu-

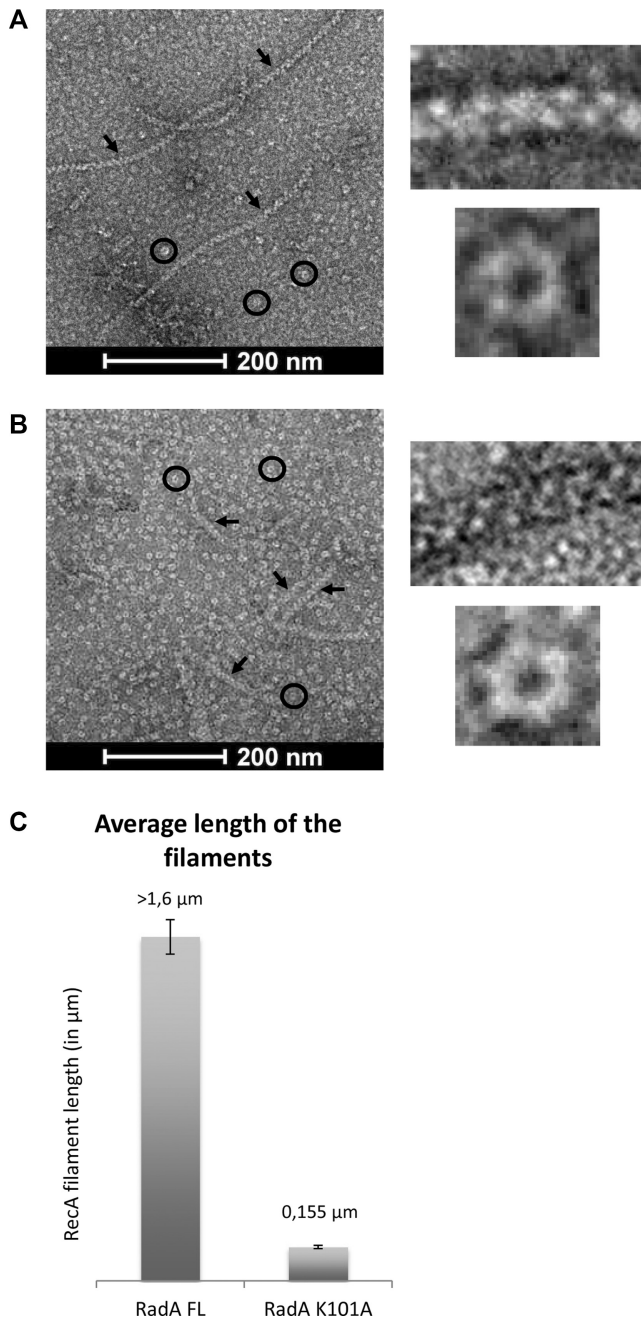


Figure 3. *SpRadA* extends *SpRecA* polymerization along ssDNA. (a and b) Negatively stained EM images of presynaptic filaments in presence of *SpRadA*_{FL} (A) and of *SpRadA*_{K101A} (B), the presynaptic filaments and *SpRadA* proteins are shown by black arrows and circles respectively. The insets on the right show a zoom of presynaptic filaments and *SpRadA*_{FL} (A), and *SpRadA*_{K101A} (B) self-assembled into ring-shaped hexamers. (C) Histogram of *SpRecA* presynaptic filaments average length in the presence of *SpRadA*_{FL} and *RadA*_{K101A}.

lar form of the M13 bacteriophage. While a few small polymers were formed in the presence of ATP in the absence of *SpRadA*, incubation of *SpRecA* with *SpRadA* in the presence of ATP γ S promoted the formation of nucleofilaments 10-fold longer than those observed with *SpRecA* alone in those conditions (Figure 3A and C). Sub-stoichiometric

amounts of *SpRadA* with respect to *SpRecA* concentration (1:4) were sufficient to generate these polymers. Observation by negative staining showed that these longer filaments formed by mixing *SpRecA* with *SpRadA* are comparable to the helical filaments generated by *SpRecA* alone, indicating that *SpRadA* promoted *SpRecA* polymerization extension along ssDNA. Next, we reproduced these experiments with *SpRadA*^{K101A} point mutant, which was previously shown to be unable to hydrolyze ATP (19). This *SpRadA*^{K101A} mutant, which still assembled into hexamers as wild-type protein (as visible on the EM grid; Figure 3B), was no longer able to promote the formation of long filaments when mixed with *SpRecA*. This result shows that ATP γ S hydrolysis is necessary to extend *SpRecA* filamentation along ssDNA. The need for *SpRadA* ATPase activity supports that it might act by translocating on the ssDNA to unwind the secondary structures that impede *SpRecA* filament growth, but without physically blocking *SpRecA* assembly on ssDNA as SSB does. However, we could not exclude that *SpRadA* assists *SpRecA* filamentation by another ATP-dependent mechanism relying on their interaction. Finally, based on this TEM analysis, we could not conclude whether *SpRadA* is associated to these nucleofilaments.

CryoEM analysis of *SpRecA* filaments assembled on ssDNA and dsDNA.

SpRecA nucleofilaments formed on long ssDNA molecules in the presence of ATP γ S are too short to allow their structural analysis by cryoEM. This drawback has been overcome via the action of *SpRadA* (see above). Long nucleoprotein filaments formed on M13 ssDNA were deposited on cryoEM Lacey grids and visualized using a 200 keV Talos Arctica cryo-electron microscope (See Supplemental Figure 2A). We used helical reconstruction in Relion to obtain a 3.9 Å resolution map. Using a non-symmetrized 3D reconstruction, we could determine in real space that these filaments display a helical symmetry and estimate the helical parameters (see Supplemental Figure 3). These helical parameters were then imposed and refined during reconstruction to obtain the final map with 15.38 Å rise and 58.46 degrees of twist (corresponding to 6.16 subunits per turn of helix) (see methods and Table 1). The final cryoEM map displayed key structural features of *SpRecA* with the bulky side chains clearly visible (Supplemental Figure 2G). A homology structural model of the *SpRecA* was obtained using Swissmodel using *EcRecA* crystal structure as template. *SpRecA* and *EcRecA* proteins share 63% identity (sequence-based alignment) and we postulated that their structure should be similar in term of secondary structure elements and overall fold. This initial model was docked into the map and the *SpRecA* structure was entirely rebuilt in our cryoEM map using coot (41). Densities for the backbone and bases of ssDNA were clearly visible. Since the sequence of M13 ssDNA is different from one filament to another, a poly-dT (thymine) DNA molecule was built in these averaged densities. Finally, ATP γ S molecules were built in the corresponding densities of the map. *SpRecA* model with ssDNA and ATP γ S was refined against the cryoEM map using real-space refinement in Phenix (34).

Table 1. Cryo-EM structure determination and model statistics for *SpRecA*-ssDNA and *SpRecA*-dsDNA complexes

Data collection	<i>SpRecA</i> -ssDNA complex	<i>SpRecA</i> -dsDNA complex
Magnification	X190 000	X120 000
Defocus range (μm)	-0.8 to -2.5	-0.8 to -2.5
Voltage (kV)	200	200
Microscope	Talos	Talos
Camera	Falcon 3	Falcon 3
Frame exposure time (s)	0.8	1
# movie frames	40	20
Total electron dose ($\text{e}^-/\text{\AA}^2$)	36	60
Pixel size (\AA)	0.76	1.24
Reconstruction	RecA-ssDNA complex	RecA-dsDNA complex
Boxe size (pixel)	180	180
Inter-box distance (\AA)	100	100
# segments extracted	363 828	1 109 194
# segments after Class2D	188 475	715 954
Resolution (\AA)	3.9	3.8
Map sharpening <i>B</i> -factor (\AA^{-2})	-141.9	-153.07
Helical rise (\AA)	15.38	14.97
Helical twist ($^\circ$)	58.46	58.62
Atomic model	RecA-ssDNA complex	RecA-dsDNA complex
Chains	9	10
# unique non-hydrogen atoms	10 381	10 515
R.m.s.d. Length (\AA)	0.006	0.007
R.m.s.d. Angles ($^\circ$)	0.993	0.963
Molprobrity score	1.84	1.86
Molprobrity clashscore, all atoms	5.10	6.90
Ramachandran outliers (%)	0	0
Ramachandran allowed (%)	10.73	7.85
Ramachandran favored (%)	89.27	92.15
Rotamer outliers (%)	0.77	0.77
C β outliers (%)	0	0
Model versus map	RecA-ssDNA complex	RecA-dsDNA complex
Correlation coefficient (mask)	0.80	0.84
Correlation coefficient (box)	0.51	0.55
Correlation coefficient (peaks)	0.25	0.25
Correlation coefficient (volume)	0.80	0.84
Correlation coefficient CC for ligands	0.80	0.87

The *SpRecA* nucleofilament structure assembled and stabilized on ssDNA with ATP γ S was found to be globally superimposable with the crystal structure of the *EcRecA*-ssDNA nucleofilament (Figure 4A and C) obtained in presence of ADP-AlF $_4$ -Mg $^{2+}$ (9). Each protomer binds to three nucleotides, organizing the ssDNA in triplets of a nearly B-form conformation that are separated from each other by 7.2 \AA (Figure 4B and D).

The structure of each *SpRecA* protomer in the nucleofilament appears to be very similar to the crystal structure of the *EcRecA* protomer unbound to DNA (9). It is composed of a N-terminal extension (residues 9–55), a typical α/β ATPase core domain (residues 56–286) containing a canonical nucleotide binding motif and the conserved DNA interacting loops L1 and L2, and a globular C-terminal domain (residues 287–341). The charged C-terminal tail (residues 342–388) could not be resolved. In the *SpRecA* filament, we numbered consecutive *SpRecA* protomers along ssDNA

in the 5' end to the 3' end direction. Within the nucleofilaments, the *SpRecA* protomers interact mostly through their ATP binding domains. In addition, the N-terminal extension of the *SpRecA*ⁿ protomer lies on the ATPase domain of the adjacent *SpRecA*ⁿ⁻¹ protomer.

Within the *SpRecA* nucleofilament, the DNA binding pockets are delineated by three consecutive *SpRecA* protomers to accommodate a DNA triplet. In each pocket, the L1 and L2 loops of *SpRecA*_n and *SpRecA*ⁿ⁺¹ protomers play a crucial role in contacting the ssDNA. Together, they encircle the DNA backbone (Figure 5A). Residues from three consecutive *SpRecA* protomers contribute to ssDNA binding through hydrogen bonds. Within the phosphate backbone of each triplet of nucleotides, from 5' to 3' end, the first phosphate group interacts with the backbone amide groups of E210 in *SpRecA*ⁿ and R226 in *SpRecA*ⁿ⁺¹, the second phosphate interacts with the backbone amide groups of G224 and G225 in *SpRecA*ⁿ⁺¹ and the third phosphate interacts with side chains from R209 in *SpRecA*ⁿ⁺¹ and S185 in *SpRecA*ⁿ⁺² (Figure 5B). The V212 residue found in the L2 loop inserts between consecutive triplets compensating the lack of base stacking in the inter-triplet junction (Figure 5B). The ATP γ S binding pocket is shared by two consecutive *SpRecA* protomers. In the *SpRecA*ⁿ protomer, the Walker A motif (residues 79–86) contacts ATP γ S with conserved residues G84, K85 and T86 contacting the ATP γ S phosphate groups (Supplemental Figure 5). The third ATP γ S phosphate makes several hydrogen bonds with the residues K265 and K267 in the RecAⁿ⁺¹, stabilizing the *SpRecA*ⁿ/*SpRecA*ⁿ⁺¹ interface. Finally, the highly conserved catalytic glutamate (E109) amongst RecA proteins is also found in the vicinity of the phosphate moieties.

The *SpRecA* filament structure is in a native conformation, without protomeric fusion. Indeed, the published crystal structure of the pre- and post-synaptic *EcRecA* filament was obtained using a chimera of six *EcRecA* protomers truncated for Nter (1–30) and Cter (336–353) residues and mutated to avoid oligomerization (C117M, S118V and Q119R). This chimera was bound to ssDNA and ADP-AlF $_4$ -Mg $^{2+}$ (9). In *SpRecA* filament, the presence of Nter or Cter regions does not modify the overall organization. When superimposed, *EcRecA* and *SpRecA* protomers have a RMSD of 1.4 \AA . Similar helical parameters are found both for *EcRecA* and *SpRecA* presynaptic filaments. Structure-based alignment shows 55.86% identity between *EcRecA* and *SpRecA* sequences. Conservation of the residues is distributed across the whole structure. The ssDNA binding pocket and the L1/L2 loops are also particularly conserved between *EcRecA* and *SpRecA*. All interactions found between ssDNA and *EcRecA* are also found in *SpRecA*. The only notable differences are the V177 and V212 residues in *SpRecA*, which correspond to the M164 and I199 residues in *EcRecA*, respectively (Figure 5C). They are located at the tip of the L2 and L1 loops, respectively. These residues belonging to two consecutive RecA protomers close the L1/L2 loops around the primary ssDNA in the pre-synaptic nucleofilament and intercalate between the DNA triplet bound to RecA. However, one marked distinction stands out. Both recombinases stretch the ssDNA molecule the B-form of DNA in a non-uniform manner, and remarkably, while the third base of each triplet was found

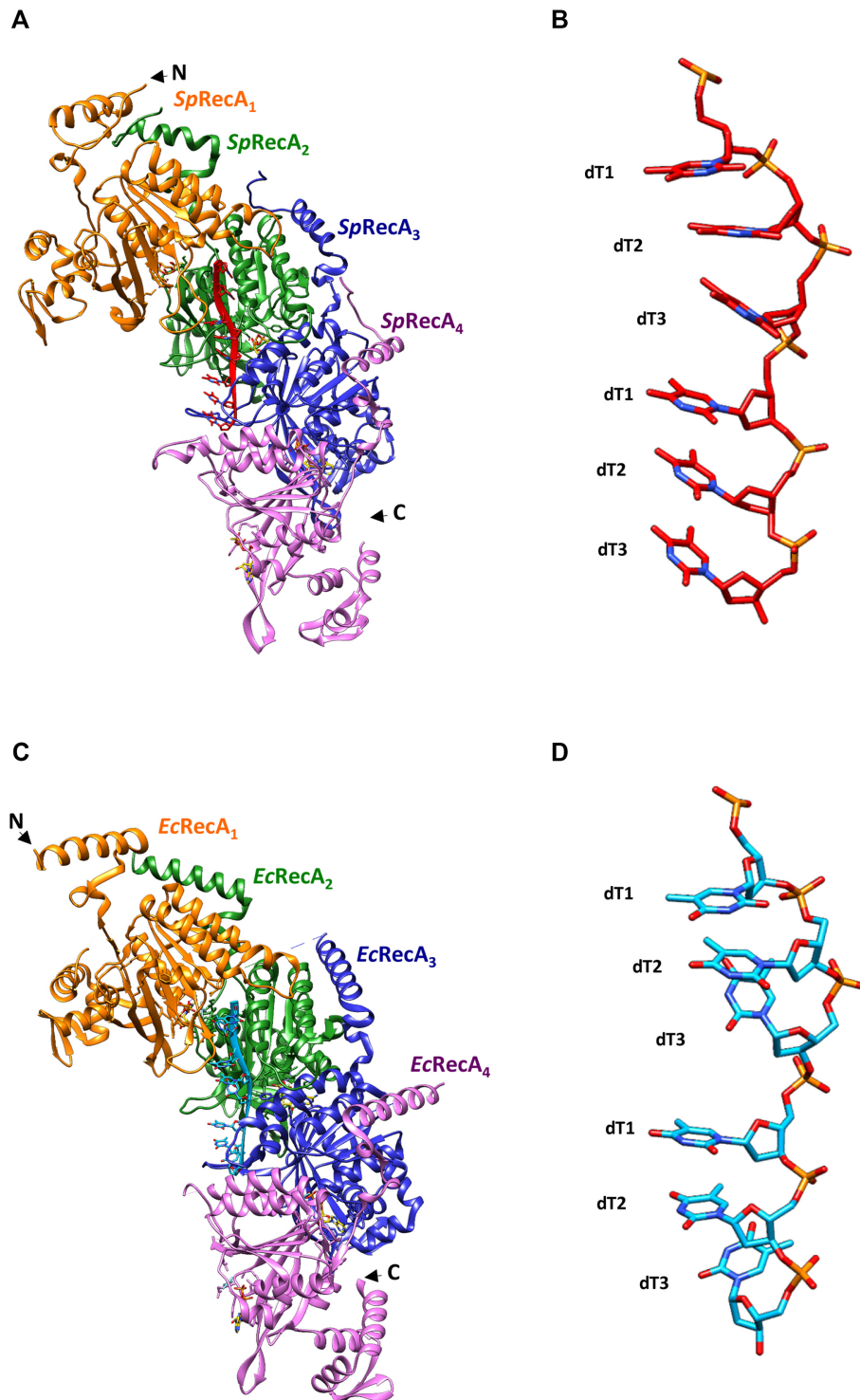


Figure 4. Structure comparison of the presynaptic nucleoprotein filaments from *Sp* and *Ec*. (A and C) Structure of the RecA–ATP γ S–dT complex from *Sp*RecA (A) and *Ec*RecA (C). Four RecA protomers are numbered from the N-terminus of the first protomer to the C-terminus of the last protomer, coloured in orange, green, blue and purple respectively. A single stranded DNA (ssDNA) molecule composed of eight thymidine nucleotides bound to *Sp*RecA and *Ec*RecA are represented in red and blue respectively. Four ATP γ S molecules are shown in gold. (B and D) Zoom on the single strand B-form DNA from *S. pneumoniae* (B) and *E. coli* (D) presynaptic filaments. The ssDNA is numbered starting with the 5'-most nucleotide in each nucleotide triplet. The ssDNA binds with a stoichiometry of exactly three nucleotides per RecA, and the repeating unit of the DNA structure is a group of three nucleotides with a 3.5–4.2 Å spacing.

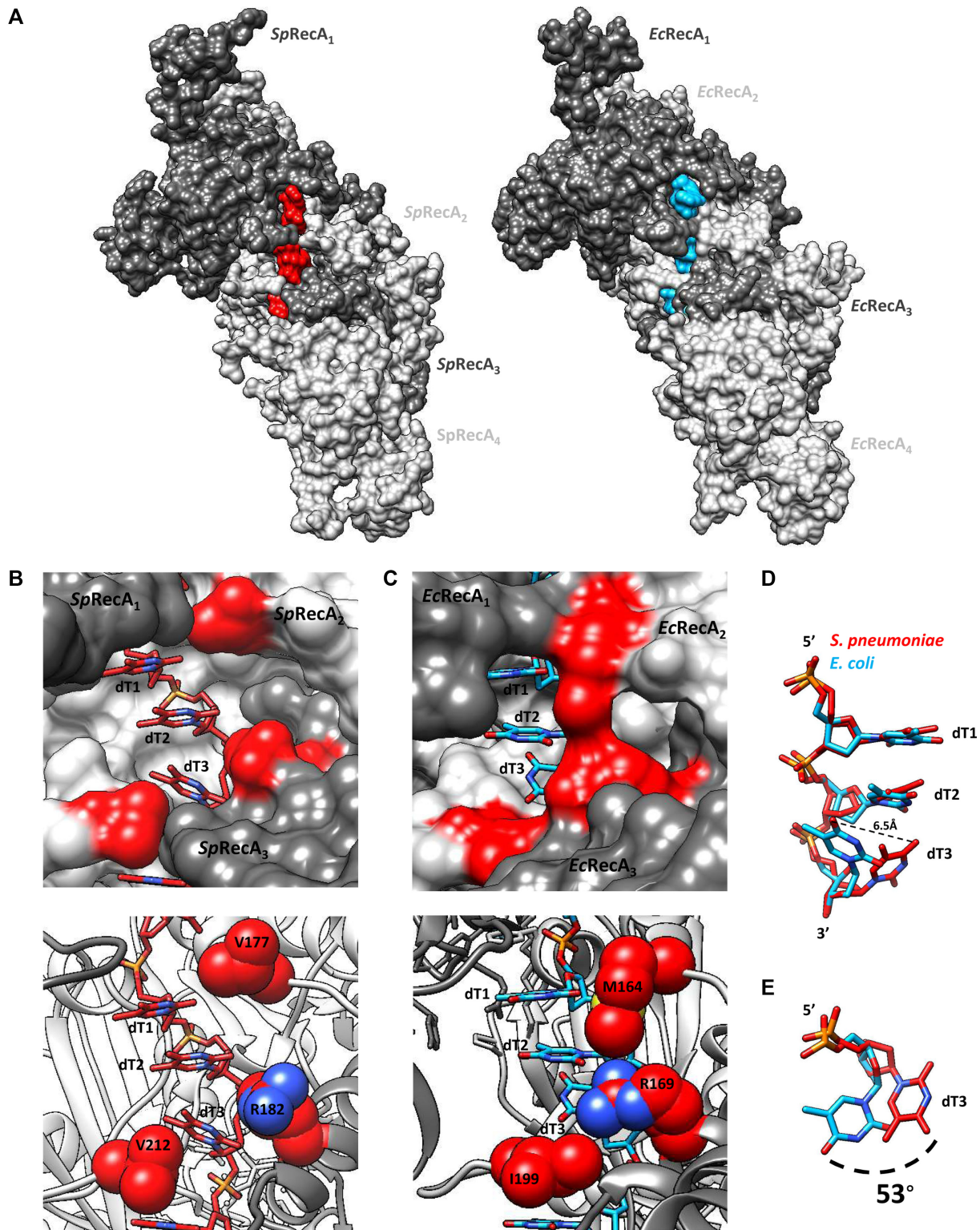


Figure 5. Interaction comparison between ssDNA and RecA protomers from *Sp* and *Ec*. (A) Surface representation comparison of the RecA-ATPyS-dT complex from *S. pneumoniae* (*SpRecA*) on the left and from *E. coli* (*EcRecA*) on the right. Four RecA protomers are numbered from the N-terminus of the first protomer to the C-terminus of the last protomer, coloured in different grey. A single stranded DNA (ssDNA) molecule composed of eight thymidine nucleotides bound to *SpRecA* and *EcRecA* are represented in red and blue respectively. (B and C) Zoom of the RecA-ssDNA contacts from *S. pneumoniae* (B) and *E. coli* (C) presynaptic filaments. Each nucleotide triplet is bound by three consecutive RecA protomers. RecA protomers and ssDNA are numbered and coloured as the Figure 4A. Residues V177, R182 and V212 from *S. pneumoniae* presynaptic filament (B) and residues M164, R169, and I199 from *E. coli* presynaptic filament (C) are coloured in red. (D) Superimposition of the nucleotide triplets bound to *SpRecA* (red) and *EcRecA* (blue). The two first nucleotides can be superimposed while the last nucleotide of each triplet shows a difference in orientation, represented by a dotted line of 6.5 Å long. (E) Top view of the last nucleotide of each triplet superimposed and numbered dT3. The superimposition shows a shift of 53°.

turned towards the interior of the *EcRecA* protein filament, the three bases of the nucleotide triplet are all aligned toward the outer surface of the *SpRecA* protein filament.

In parallel, we analyzed *SpRecA* filamentation on dsDNA and, by contrast with the ssDNA matrix, we found that *SpRecA* could self-assemble on dsDNA into long and stable filaments in the presence of ATP γ S. We successfully analyzed their structure by cryoEM by applying a similar procedure as with filaments obtained on ssDNA. A 3.8 Å resolution map of these filaments has been obtained, in which we built and refined the structure of *SpRecA* bound to dsDNA and ATP γ S with a helical symmetry of 14.97 Å rise and 58.62 Å twist (corresponding to 6.14 subunits per turn). The overall structure of the individual *SpRecA* protomer, as well as the interactions between *SpRecA* protomers and with the ATP γ S in this filament assembled on dsDNA are identical to those characterized for the filament assembled on ssDNA (Supplemental Figure 2B). Remarkably, however, the overall dsDNA B-form structure has been notably modified by polymerization of *SpRecA* protomers. These were found to interact with one DNA strand as in the filament built with ssDNA. The complementary strand makes very few contacts with *SpRecA* protomers (Supplemental Figure 4). Like in *EcRecA* filaments, we propose that this strand interacts with this primary DNA strand through Watson–Crick hydrogen bonds. Interestingly, this structural organization of the dsDNA generated by *SpRecA* polymerization appeared to be identical to the crystal structure of the dsDNA molecule resulting from the pairing of a ssDNA strand pre-bound by *EcRecA* with its complementary ssDNA strand (9).

Direct imaging of *SpRecA* assembly on single molecules of DNA by TIRFm.

Next, we undertook the analysis of nucleofilamentation dynamics of *SpRecA*. To this end, we performed real-time observation of its polymerization on a single DNA molecule by Total Internal Reflection Fluorescence microscopy (TIRFm), following the same procedure previously developed for the study of *EcRecA* nucleofilamentation (27). We used a DNA substrate composed of a central ssDNA gap of 8155 nucleotides flanked by biotinylated dsDNA ‘handles’ of 21 080 and 24 590 bp (Figure 6A) and a fluorescently labeled *SpRecA* (Alexa 488, named *SpRecA*^{A488} hereafter) characterized for several activities. The purified labeled *SpRecA*^{A488} was demonstrated to be active for ssDNA binding, D-loop formation and ssDNA-dependent ATP hydrolysis with a slight defect compared to the non-labeled protein (Supplemental Figure 6). DNA molecules were then attached to the surface of a streptavidin-coated glass coverslip in a microfluidic chamber and visualized by TIRFm. We detected interaction of *SpRecA*^{A488} with DNA in the presence of ATP γ S, but not with ATP, reproducing our previous TEM experiments (Figure 1D). *SpRecA* filament formation first appeared as a single spot in the minute range.

Then, the size of individual *SpRecA*^{A488} filaments gradually grew over time (Figure 6B) to reach a stable length after 15 min. The final filament occupies the place on the DNA molecule that is unbound by Sytox and, therefore,

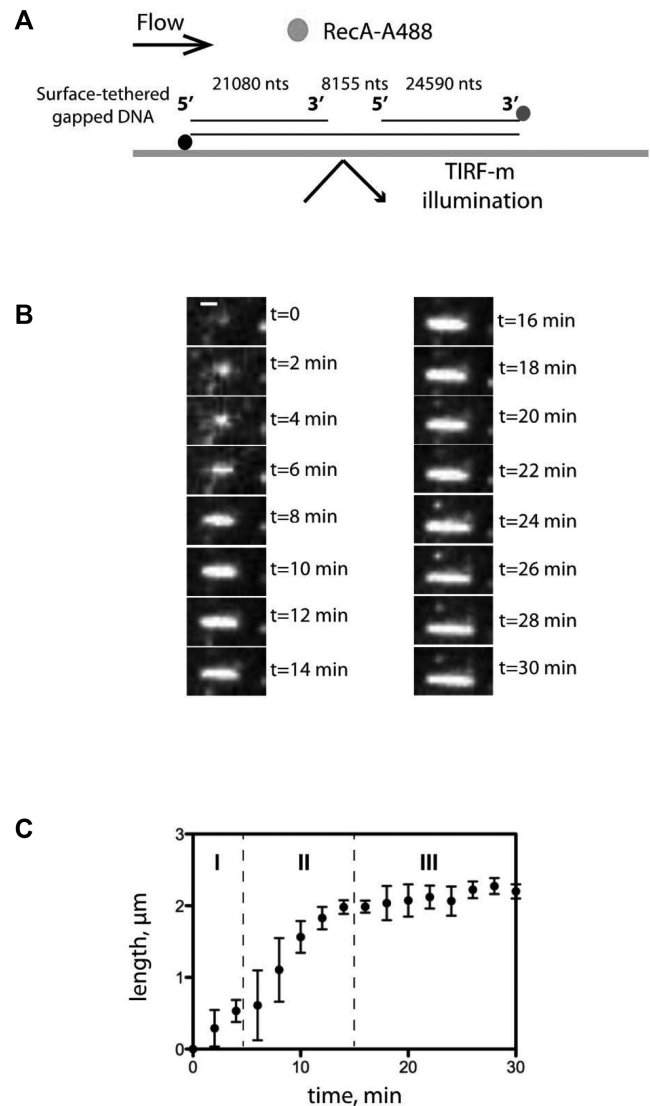


Figure 6. TIRFm analysis of *SpRecA* assembly on single molecules of ssDNA. (A) Schematic of the experimental set up combining TIRFm and microfluidics for direct imaging of *SpRecA*^{A488} filament assembly in presence of ATP γ S on a single molecule of ssDNA tethered within a microfluidic flow chamber. (B) Sequential images of *SpRecA*^{A488} filament assembly in presence of ATP γ S. Scale bars represent 1 μ m and the time interval in min (min) is indicated in the images. (C) The length of *SpRecA*^{A488} filament clusters increases linearly with time. The plots are the average of three experiments and the standard error of the mean (sem) is represented.

corresponds to the ssDNA portion. The averaged *SpRecA* filament growth rate measured on three individual DNA molecules showed a consistent and reproducible polymerization into three distinct stages, referred to as initiation, elongation, termination (Figure 6C). The elongation rate of *SpRecA* nucleofilament was $165 \pm 18 \text{ nm min}^{-1}$, which is similar to the elongation rate previously reported measured for *EcRecA* and measured on the same DNA molecule ($50\text{--}500 \text{ nm min}^{-1}$, Bell *et al.*, 2012). The *SpRecA*^{A488} filament assembly eventually reached a stable and maximum length of $2.1 \pm 0.1 \mu\text{m}$, which is 10–20-fold longer than *SpRecA* nucleofilaments measured by TEM in the experimental conditions of TEM (compare Figure 2C and Figure 3).

However, this measured length of the nucleofilament does not correspond to the maximum length of 4 μm expected for a saturating coverage of the ssDNA portion of the DNA substrate by one RecA molecule every 3 nucleotides (as demonstrated with the solved cryoEM structure of the *SpRecA* nucleofilament; Figure 4).

Altogether, this TIRFm analysis shows that *SpRecA* filament growth follows the same dynamics as that reported for *EcRecA*. The two recombinases appear to differ in their intrinsic capacity to overcome some secondary structures to extend along the ssDNA matrix, but not in their elongation rate along ssDNA.

***SpRecA* ATP-dependent ssDNA binding mode**

As we were not able to detect any *SpRecA* assembly on DNA by TIRFm in the presence of ATP, we used Fluorescence Correlation Spectroscopy (FCS) and Fluorescence Anisotropy (FA) to measure the kinetics of formation of short *SpRecA* polymers on ssDNA that could not have been detected by TIRF microscopy.

FCS allows the detection of fluorescently labeled molecules that diffuse through a sub-femtoliter detection volume, giving rise to intensity fluctuations in real time and at the millisecond scale (Figure 7A) and allowing to calculate their diffusion time within the observation volume τ_D . We used ssDNA substrates with random sequences, labeled with Alexa 488 at the 5' end. We tested several lengths of ssDNA substrates, i.e. 1000, 500 and 100 nucleotides long, and we were able to detect exploitable signal changes only for the small 100-mers. Upon addition of *SpRecA* or *EcRecA* and ATP, the diffusion time increased with time prior reaching a plateau that reports on the ssDNA assembly kinetics of the two recombinases (Figure 7B and C, for 250 and 400 nM of each RecA, respectively). Thus, in these conditions, we were able to detect *SpRecA* and *EcRecA* assembly on ssDNA in the presence of hydrolysable ATP and to compare their kinetics in those conditions. To this end, we measured the average half-time to reach the plateau value in each condition. This was slightly shorter for *SpRecA* in both conditions, i.e. 72 s for *SpRecA* and 112 s for *EcRecA* at 250 nM, and 69 s for *SpRecA* and 132 s for *EcRecA* at 400 nM. In addition, the kinetics of assembly on ssDNA appeared to be clearly different for the two recombinases. Indeed, in the very early stage of *EcRecA* assembly (Figure 7, blue curve, zoom), the curve showed a cooperative mode, whereas *SpRecA* assembly was faster and showed no cooperativity.

In these FCS experiments, ATP hydrolysis by both recombinases triggered by their binding to ssDNA does not impact the stability of their interaction on ssDNA during such short periods of time. Complementarily, we characterized ssDNA binding affinity of *SpRecA* and *EcRecA* protein at steady state. To this end, we measured by fluorescence anisotropy (FA) their apparent affinities constants for a short 65 nucleotides long fluorescent ssDNA molecule (T65). FA measurements were performed at 0.1 mM and 1 mM ATP, in large excess compared to the *EcRecA* and *SpRecA* concentrations used (Figure 7D and E, respectively). In those conditions, the measured apparent affinity for ssDNA (Kd) was 6- to 2-fold lower for *SpRecA*

than for *EcRecA* at 0.1 mM ATP and 1 mM of ATP, respectively (Figure 7H). In addition, the maximum FA value reached -0.26 for *EcRecA*, whereas it was <0.2 for *SpRecA*, pointing at a different apparent molecular size or folding of the nucleoprotein complexes. Thus, while the FCS analysis demonstrates that the two recombinases present a nearly equivalent half-time of association on ssDNA in the presence of ATP, the FA analysis indicates that they display a different ssDNA binding mode. Notably, no difference in the binding of *EcRecA* to ssDNA was observed at the two ATP concentrations tested. In marked contrast, the plateau value reached for *SpRecA* was found to be lower at 0.1 mM than at 1 mM ATP, and this latter value was lower than the one measured for *EcRecA*. To test the impact of ATP hydrolysis in these differences, we reproduced these FA experiments in the presence of ATP γ S or ATP-BeF₃. Interestingly, in those conditions the ssDNA binding curves obtained for *SpRecA* were found identical whatever nucleotide concentration used, either 0.1 or 1 mM and the value of the plateau matched with *EcRecA* curves generated in the presence of ATP (Figures 7F and G to compare with 7D). This FA analysis showed that ATP hydrolysis modulates differently *SpRecA* and *EcRecA* interaction on ssDNA, despite both exhibit a similar ssDNA-induced ATP hydrolysis rate (Supplemental Figure 7). Altogether, these results show that *SpRecA* binding on ssDNA appears markedly less stable upon ATP hydrolysis, pointing at a distinct and more dynamic mode of interaction with ssDNA for *SpRecA* in comparison with that of *EcRecA*. Also, ssDNA binding activities of both RecA proteins measured by FCS and FA revealed that ATP hydrolysis impacts differently the stability of their interaction on ssDNA, while they display a similar rate of ssDNA-dependent ATP hydrolysis.

***SpRecA* is more efficient than *EcRecA* in a D-loop assay.**

Then, we measured the intrinsic ATP-dependent DNA strand-exchange activity of *SpRecA* and *EcRecA*. To this end, we used the D-loop assay illustrated in Figure 8b. In this assay, a 100-nucleotides (nts) linear oligonucleotide, fluorescently labeled with Cy3 at its 5' end, was incubated with increasing amounts of *SpRecA* or *EcRecA* and mixed with a homologous supercoiled plasmid. Following protein denaturation, the fluorescent D-loop product was separated from free ssDNA by agarose gel electrophoresis and quantified. *SpRecA* was found to be up to three times more efficient than *EcRecA* ($3.1\% \pm 1.15$ versus $1.29\% \pm 0.57$, respectively; Figure 1C). This result contrasts with a previous analysis reporting a less efficient HR activity of *SpRecA* in comparison with *EcRecA* when similarly tested alone in the presence of ATP (40). However, the HR assay used was markedly different. In this former assay depicted in Figure 8A, the HR reaction is initiated by DNA strand exchange at one end of a linear dsDNA molecule with its complementary sequence on a long circular homologous ssDNA molecule (>5000 nts) and is followed by DNA branch migration over a long distance to get the final product. By contrast, the D-loop product results from the invasive pairing between a short ssDNA molecule with its complementary sequence in a supercoiled dsDNA molecule. Thus, *SpRecA* and *EcRecA* appear to be oppositely and differently active

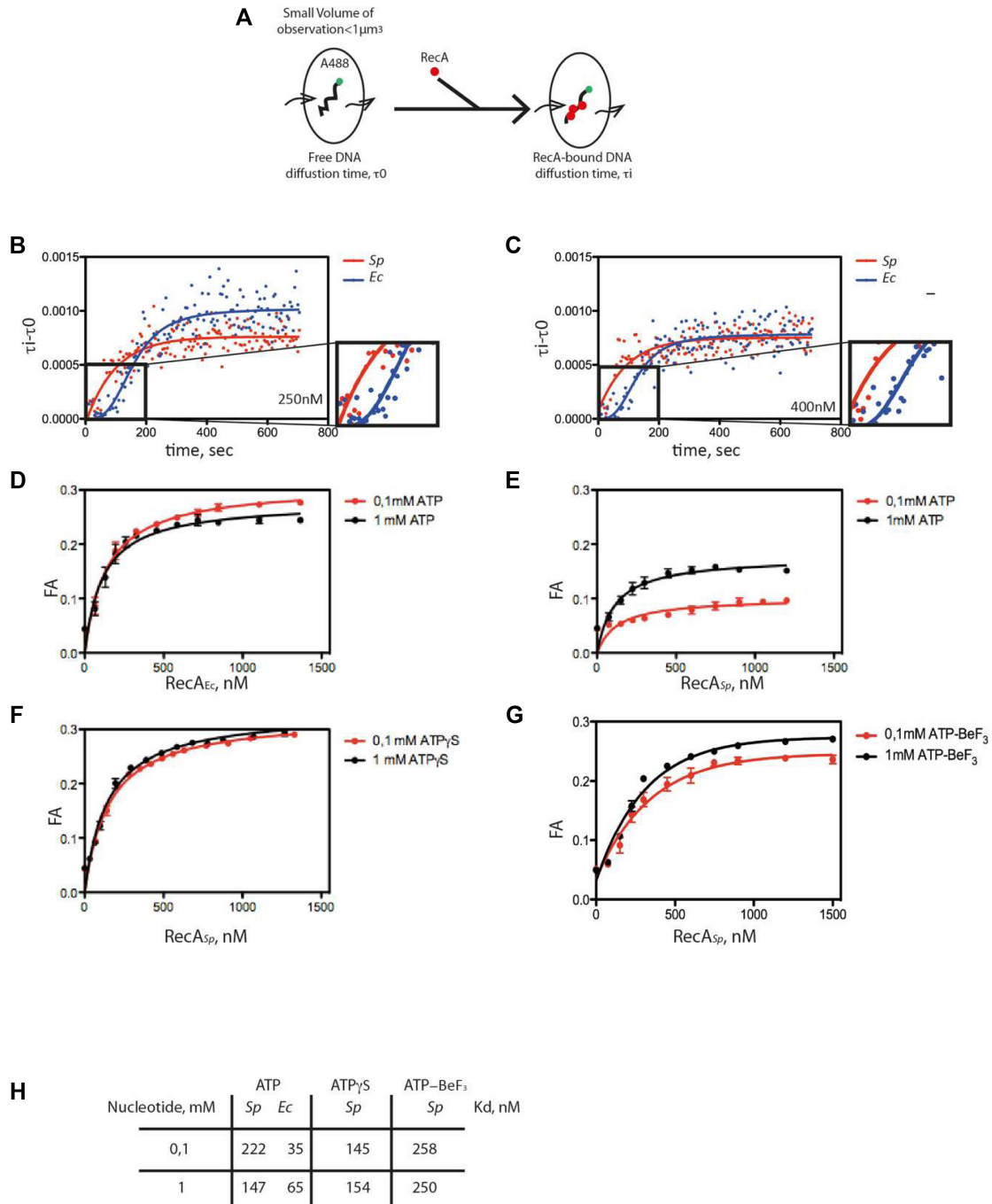


Figure 7. FCS analysis of *Sp*RecA and *Ec*RecA assembly on single molecules of ssDNA. (A) Schematic of the experimental set up using FCS for the direct measurement of the change of diffusion time of fluorescently labeled (A488) ssDNA of 100 nucleotides length upon binding of *Sp*RecA and *Ec*RecA. (B and C) Averaged curve of three measurements of diffusion time at 250 nM of protein (B) showing a mean of half-time polymerization of 72.54 ± 11.85 s for *Sp*RecA and 111.99 ± 18.24 s for *Ec*RecA and at 400 nM of protein (C) showing a mean of half-time polymerization of 69 ± 6.0 s for *Sp*RecA and $132, 35 \pm 29.8$ s for *Ec*RecA. (D–H) Equilibrium binding of *Ec*RecA (D) of *Sp*RecA (E) of *Ec*RecA in the presence of ATP. Fluorescence anisotropy (FA) variation with 1 mM ATP (black circles) and 0.1 mM ATP (red circles) with a K_d of 65 nM and 35 nM in presence of 1 mM and 0.1 mM ATP, respectively. The plots are the average of three experiments and the standard error of the mean (sem) is represented. In the presence of ATP γ S (F); ATP-BeF₃ (G); parameters table (K_d) obtained from the above measurements (H).

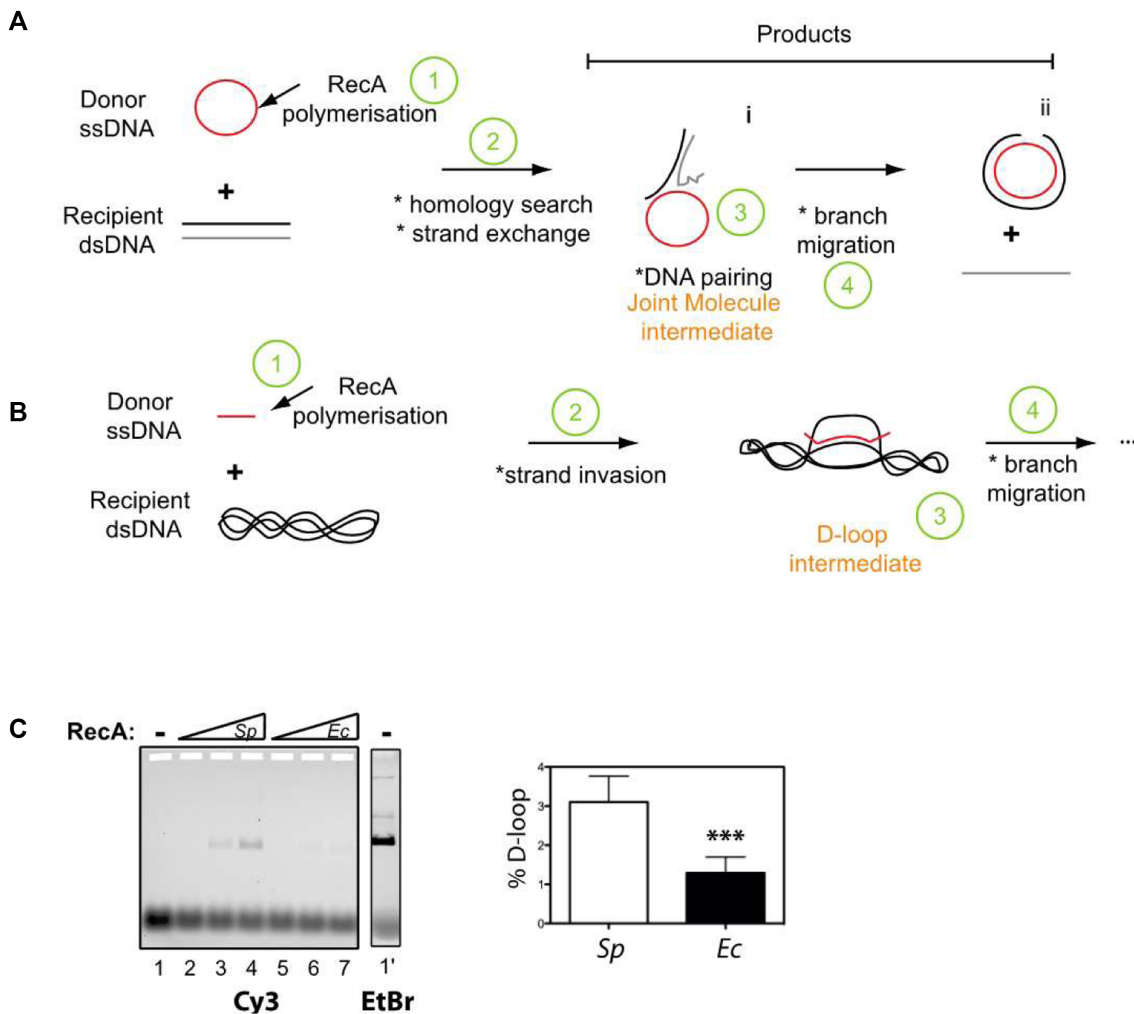


Figure 8. Comparison of *SpRecA* and *EcRecA* recombination activity in a D-loop assay. (A and B) Schematics of *in vitro* DNA strands exchange assays commonly used to measure the recombination activity of HR recombinases; the D-loop assay is depicted in (B). (C) Left: deproteinized agarose gel of the D-loop reaction performed in presence of 10 nM of cy3 oligonucleotide (100 mers) 5 nM (1 ml) of pUC18 vector, and increased amount (150–600 nM) of *SpRecA* or *EcRecA* as indicated above the gel (*Sp* and *Ec*, respectively). Right: quantification of the D-loop product generated at 600 nM of *SpRecA* and *EcRecA* concentration. The percentage of D-loop formed is given as mean values \pm standard error of the mean (sem) of three reactions.

in catalyzing the initial ssDNA pairing with a complementary sequence and in extending ssDNA recombination by DNA branch migration. Altogether, these functional divergences between these two bacterial RecA appear to stem from the different stability of their presynaptic filaments independent of the ATP hydrolysis rate.

DISCUSSION

We report a comprehensive molecular study of *SpRecA* functional properties, which provides important insights into its DNA interaction properties in relation with its DNA strand exchange activities. This *in vitro* analysis shows that *SpRecA* markedly differs from the *EcRecA* paradigm in the early stages of HR. Our findings collectively concur to the conclusion that the main deviation between the two HR recombinases mostly stems from their ATP-dependent ssDNA binding mode and independently of their ATPase rates. Our studies also highlight the lack of synergy between *SpRecA* and its two cognate and paralogous SSB proteins

in elongating its presynaptic filamentation. We found that *SpRecA* filamentation on ssDNA could be assisted by the conserved RadaA helicase, previously known to act coordinately with RecA on postsynaptic HR intermediates (1,2). In addition, our findings support a model of HR mechanism in which the *SpRecA* presynaptic filament would be more efficient than *EcRecA* in homology search and ssDNA pairing within a recipient complementary dsDNA molecule.

Key variations in the ATP-dependent ssDNA interaction dynamics of *SpRecA* and *EcRecA*.

A central intermediate of the HR mechanism is the presynaptic filament, which is dynamically assembled and disassembled on ssDNA by ATP binding and hydrolysis between the protomers of the recombinase (3). This ssDNA-dependent ATP cycle is not uniformly conserved between bacterial RecA, leading to various lengths of presynaptic filaments (1,42). We report here that *SpRecA* interac-

tion with ssDNA in the presence of ATP evaluated by FA analysis is more dynamic than that of *EcRecA* (Figure 7). These results are consistent with previous studies showing in *SpRecA* biochemical assays an enhanced ssDNA binding and DNA strand exchange activities in the presence of dATP or ATP γ S instead of ATP (42,48). This finding indicates that *SpRecA* forms shorter nucleofilaments than *EcRecA*, as further supported by TEM analysis (Figure 1). However, this marked difference between the two recombinases is not due to a different affinity for ATP, nor to a different ssDNA-dependent ATP hydrolysis rate, nor to a different kinetic in ATP-dependent interaction with ssDNA (Supplemental figure 7) (48). Thus, a possible cause of the limited extension of the presynaptic filament of *SpRecA* would be a lower binding stability of its protomers on ssDNA. Within the HR presynaptic filament, each protomer interacting with ssDNA is further stabilized *via* interaction with two adjacent protomers through ATP binding (43). Upon ATP hydrolysis, protomers located at the tips of the filament are less stably bound to ssDNA, as they are engaged in only one interaction with an adjacent protomer. Thus, it has been shown by biochemical and SM analysis that the ATP-*EcRecA* filament mainly disassembles at the 5' side and grows in the 3' direction of the ssDNA (44). In direct line with such a polymerization dynamic, the 5' terminal protomer of the *SpRecA* filament might be less stable on ssDNA upon ATP hydrolysis than in the case of the *EcRecA* filament. In addition, the release of Pi from the ADP-Pi product will change the interactions between the two protomers, which will alter their interaction with ssDNA. Thus, a possible source of difference between *SpRecA* and *EcRecA* impacting the length of their presynaptic filaments would be the ADP-Pi release and/or ATP turnover at the interface of two protomers bound to ssDNA.

Furthermore, even under stabilizing conditions that restrain ATP hydrolysis (with the use of ATP γ S or by adding BeF3 to ATP), *SpRecA* appears less prone than *EcRecA* to elongate on ssDNA (Figure 1). We interpret this difference as a lower capability of *SpRecA* to melt ssDNA secondary structures in comparison with *EcRecA*, limiting differentially their filament growth. The longer *SpRecA* presynaptic filaments observed in TIRFm than in TEM experiments supports this proposal (Figures 2 and 3). SM observation of *SpRecA* filamentation by TIRFm is performed in real time in a microfluidic chamber on an attached DNA molecule and under flux, which will physically extend the ssDNA and limit its self-pairing into secondary structures. As a result, *SpRecA* could extend its polymerization, stabilized by limiting ATP hydrolysis, on a longer distance than on an unstretched ssDNA molecule as in the TEM experiments.

Another distinct ssDNA interaction property between these two recombinases has been uncovered from the characterization by cryoEM of the *SpRecA* nucleofilament structure stabilized by ATP γ S. This structure is superimposed to a large extent on the *EcRecA* filament resolved by crystallization (9). In both *SpRecA* and *EcRecA* nucleofilaments, the ssDNA molecule is bound into an identical helical and extended conformation organized in triplets of nu-

cleotides. However, the 3 bases of each triplet of nucleotides are fully exposed toward the exterior in the *SpRecA* filament, contrasting with the *EcRecA* filament where the third base of each nucleotide triplet is flipped inward (9). These characteristics suggest that the ssDNA conformation in the *SpRecA* filament is potentially more favorable for the homology search.

Lack of SSB assistance in the extension of *SpRecA* presynaptic filamentation.

One of the key roles of SSB in the early HR steps is to assist presynaptic filament extension by melting out ssDNA secondary structures (17). This interplay originally characterized between RecA and SSB of *E. coli* has been generalized to RecA of many other species, with some exceptions such as for *SpRecA* or *B. subtilis* RecA (45). Indeed, either of the two pneumococcal SsbA and SsbB proteins, or *EcSSB* were found to inhibit *SpRecA* binding to ssDNA, as deduced from their inhibition of the ssDNA dependent *SpRecA* ATPase activity (25). Here, we directly observed by TEM analysis that any of these SSB outcompetes ATP-dependent *SpRecA* polymerization on long ssDNA molecules. Furthermore, their addition to the short *SpRecA* filaments stabilized by ATP γ S simply conduct to their binding on ssDNA portions unbound by *SpRecA*, without promoting the extension of *SpRecA* nucleofilaments as in the case of *EcRecA* (Figure 2). This result firmly demonstrated the lack of assistance by any SSB in elongating *SpRecA* polymers on ssDNA. They also indicate that the inhibition by SSB proteins of the ATP-dependent *SpRecA* interaction on ssDNA is the result of a more stable binding of SSB in comparison to the highly dynamic binding of *SpRecA*, leading to a full occupancy of the ssDNA by SSB in these conditions. This also shows that SSB can bind to ssDNA parts that are inaccessible to *SpRecA* and inferred to be secondary structures.

An elegant genetic screen of *EcRecA* mutants more efficient in conjugational recombination resulted in the selection of several point mutants that were all found to exhibit *in vitro* a greater persistence on ssDNA and a more efficient displacement of SSB than wild type *EcRecA* (46). The *EcRecA* region randomly mutated in this screening corresponds to the large N-ter region involved in RecA subunit-subunit interaction. This shows that modulations in this interacting interface could impact the intrinsic ssDNA interacting and polymerizing property of RecA on ssDNA. However, comparison of this interaction surface between *SpRecA* and *EcRecA* could not highlight a particular difference that would explain the lower persistence of *SpRecA* on ssDNA that we report here (Supplemental Figure 8). In addition, other subtle variations between RecA proteins might influence their intrinsic stability on ssDNA. Indeed, another possible source of variation could be the residues engaged in direct interaction with ssDNA, as we found here in the structure of the presynaptic filaments of *SpRecA* in comparison with *EcRecA* (see above). However, further studies are needed to establish whether this different organization of the presynaptic filament modifies their dynamism.

An unprecedented role of the RadA HR effector in extending RecA presynaptic filamentation.

The less stable ssDNA binding in *SpRecA* filament leads to their limited extension, which is impeded by SSB proteins or ssDNA secondary structures and unfavorable for the branch migration step in HR reaction (25). SSB proteins are well known effectors that assist RecA dynamics and filament length (47). For *E. coli*, *Pseudomonas aeruginosa*, *Neisseria gonorrhoeae*, *Herbaspirillum seropedicae* or *Bacillus subtilis* (*Bs*) RecA proteins, SSB proteins remove structures in ssDNA to facilitate formation of *EcRecA* nucleoprotein filaments on ssDNA (48). In the experimental conditions tested here, *SpSsbA* or *SpSsbB* protein improve only very slightly or compete with the *SpRecA* filament extension. Like for *DrRecA*, *SpRecA* ATP hydrolysis is inhibited by *SpSsbA* or *EcSSB*. So, regarding SSB proteins, *SpRecA* showed a distinct behavior shared with *DrRecA*. In contrast, *SpRadA* helicase enhanced the *SpRecA* filament extension. It does so without co-polymerizing with it. The use of the ATP hydrolysis mutant of *SpRadA* (*SpRadA*^{K101A}) showed that the ATP hydrolysis activity of *SpRadA* is required to enhance *SpRecA* filament extension. This strongly suggests that helicase activity of *SpRadA* could remove ssDNA secondary structures to help *SpRecA* extension. Interestingly, RecA filament growth is well known to proceed from 5' to 3' on ssDNA, which is also the translocation directionality of *SpRadA* when acting as helicase (19). Thus, *SpRadA* not only acts in HR mechanism at the post-synaptic step by promoting DNA branch migration (5,18,19) but also at the presynaptic step, by relieving the stem-loop structures that form on ssDNA and that impede RecA polymerization. Interestingly, *SpRecA* is markedly inefficient in directing these two HR steps by itself (this study; (25)). By marked contrast, we found that *SpRecA* is intrinsically highly efficient in promoting homologous ssDNA pairing in dsDNA template, even more than the *EcRecA* paradigm (Figure 8C).

Altogether, this detailed structural and biochemical analysis of ATP-dependent DNA interacting properties of *SpRecA* points at their balanced intrinsic efficiency by comparison with the *EcRecA* paradigm. Also, these activities could be differently compensated by accessory effectors. These key variations on the conserved RecA-directed HR mechanism points at its adaptation amongst bacterial species, which could reflect specific needs and/or its particular integration with other processes at work on their genome.

DATA AVAILABILITY

The cryo-EM densities of RecA nucleofilaments on ssDNA and dsDNA have been deposited in the Electron Microscopy Data Bank under ID codes EMD-15524 and EMD-15525 respectively. The models for RecA nucleofilaments on ssDNA and dsDNA have been deposited in the PDB under ID codes PDB 8AMD and 8AMF respectively. Raw cryo-EM data are available on request.

SUPPLEMENTARY DATA

Supplementary Data are available at NAR Online.

FUNDING

Centre National de la Recherche Scientifique, University Paul Sabatier; Agence Nationale de la Recherche [ANR-10-BLAN-1331]; IdEX Toulouse funding for Emergence with the SMART project 'Single Molecule Analysis of Homologous Recombination' attributed to M.H. and for Equipment with the 'Go ahead in life sciences in Toulouse' project; Fondation pour la Recherche Médicale (FRM) [ING20150532556] for the salary of S.S.; European Research Council (ERC) consolidator grant TransfoPneumo (725554) attributed to R.F.; S.C.K. was supported by grants from NIH (GM62653, GM64745, and R35 GM131900) and DOD-CDMRP (BC171869); France Bio Imaging (FBI) funding attributed to E.M. & M.H.; We thank Chantal Prevost for helpful discussions. Funding for open access charge: ERC PneumoTransfo.

Conflict of interest statement. None declared.

REFERENCES

- Cox, M.M. (2007) Regulation of bacterial RecA protein function. *Crit. Rev. Biochem. Mol. Biol.*, **42**, 41–63.
- Bell, J.C. and Kowalczykowski, S.C. (2016) Mechanics and single-molecule interrogation of DNA recombination. *Annu. Rev. Biochem.*, **85**, 193–226.
- Liu, J., Ehmsen, K.T., Heyer, W.-D. and Morrical, S.W. (2011) Presynaptic filament dynamics in homologous recombination and DNA repair. *Crit. Rev. Biochem. Mol. Biol.*, **46**, 240–270.
- Michel, B. and Leach, D. (2012) Homologous recombination—enzymes and pathways. *EcoSal Plus*, **5**, <https://doi.org/10.1128/ecosalplus.7.2.7>.
- Cooper, D.L. and Lovett, S.T. (2016) Recombinational branch migration by the RadA/Sms paralog of RecA in *Escherichia coli*. *Elife*, **5**, e10807.
- Kowalczykowski, S.C. (2015) An overview of the molecular mechanisms of recombinational DNA repair. *Cold Spring Harb. Perspect. Biol.*, **7**, a016410.
- Renkawitz, J., Lademann, C.A. and Jentsch, S. (2014) Mechanisms and principles of homology search during recombination. *Nat. Rev. Mol. Cell Biol.*, **15**, 369–383.
- Del Val, E., Nasser, W., Abaibou, H. and Reverchon, S. (2019) RecA and DNA recombination: a review of molecular mechanisms. *Biochem. Soc. Trans.*, **47**, 1511–1531.
- Chen, Z., Yang, H. and Pavletich, N.P. (2008) Mechanism of homologous recombination from the RecA-ssDNA/dsDNA structures. *Nature*, **453**, 489–484.
- Yang, H., Zhou, C., Dhar, A. and Pavletich, N.P. (2020) Mechanism of strand exchange from RecA-DNA synaptic and D-loop structures. *Nature*, **586**, 801–806.
- Lin, Y.H., Chu, C.C., Fan, H.F., Wang, P.Y., Cox, M.M. and Li, H.W. (2019) A 5'-to-3' strand exchange polarity is intrinsic to RecA nucleoprotein filaments in the absence of ATP hydrolysis. *Nucleic Acids Res.*, **47**, 5126–5140.
- Konforti, B.B. and Davis, R.W. (1990) The preference for a 3' homologous end is intrinsic to RecA-promoted strand exchange. *J. Biol. Chem.*, **265**, 6916–6920.
- Konforti, B.B. and Davis, R.W. (1992) ATP hydrolysis and the displaced strand are two factors that determine the polarity of RecA-promoted DNA strand exchange. *J. Mol. Biol.*, **227**, 38–53.
- Joo, C., McKinney, S.A., Nakamura, M., Rasnik, I., Myong, S. and Ha, T. (2006) Real-time observation of RecA filament dynamics with single monomer resolution. *Cell*, **126**, 515–527.
- Lee, J.Y., Terakawa, T., Qi, Z., Steinfeld, J.B., Redding, S., Kwon, Y., Gaines, W.A., Zhao, W., Sung, P. and Greene, E.C. (2015) DNA recom. Base triplet stepping by the Rad51/RecA family of recombinases. *Science*, **349**, 977–981.
- Antony, E. and Lohman, T.M. (2019) Dynamics of *E. coli* single stranded DNA binding (SSB) protein-DNA complexes. *Semin. Cell Dev. Biol.*, **86**, 102–111.

17. Bianco,P.R. (2017) The tale of SSB. *Prog. Biophys. Mol. Biol.*, **127**, 111–118.
18. Torres,R., Serrano,E. and Alonso,J.C. (2019) Bacillus subtilis RecA interacts with and loads RadA/Sms to unwind recombination intermediates during natural chromosomal transformation. *Nucleic Acids Res.*, **47**, 9198–9215.
19. Marie,L., Rapisarda,C., Morales,V., Bergé,M., Perry,T., Soulet,A.-L., Gruget,C., Remaut,H., Fronzes,R. and Polard,P. (2017) Bacterial RadA is a DnaB-type helicase interacting with RecA to promote bidirectional D-loop extension. *Nat. Commun.*, **8**, 15638.
20. Baitin,D.M., Bakhlanova,I.V., Kil,Y.V., Cox,M.M. and Lanzov,V.A. (2006) Distinguishing characteristics of hyperrecombinogenic RecA protein from *Pseudomonas aeruginosa* acting in *Escherichia coli*. *J. Bacteriol.*, **188**, 5812–5820.
21. Cox,M.M. and Battista,J.R. (2005) Deinococcus radiodurans - the consummate survivor. *Nat. Rev. Microbiol.*, **3**, 882–892.
22. Johnston,C., Martin,B., Fichant,G., Polard,P. and Claverys,J.-P. (2014) Bacterial transformation: distribution, shared mechanisms and divergent control. *Nat. Rev. Microbiol.*, **12**, 181–196.
23. Steffen,S.E. and Bryant,F.R. (2001) Purification and characterization of the single-stranded DNA binding protein from *Streptococcus pneumoniae*. *Arch. Biochem. Biophys.*, **388**, 165–170.
24. Attaiech,L., Olivier,A., Mortier-Barrière,I., Soulet,A.-L., Granadel,C., Martin,B., Polard,P. and Claverys,J.-P. (2011) Role of the single-stranded DNA-binding protein SsbB in pneumococcal transformation: maintenance of a reservoir for genetic plasticity. *PLoS Genet.*, **7**, e1002156.
25. Grove,D.E. and Bryant,F.R. (2006) Effect of Mg²⁺ on the DNA binding modes of the *Streptococcus pneumoniae* SsbA and SsbB proteins. *J. Biol. Chem.*, **281**, 2087–2094.
26. Dupaigne,P., Le Breton,C., Fabre,F., Gangloff,S., Le Cam,E. and Veaute,X. (2008) The Srs2 helicase activity is stimulated by Rad51 filaments on dsDNA: implications for crossover incidence during mitotic recombination. *Mol. Cell.*, **29**, 243–254.
27. Bell,J.C., Plank,J.L., Dombrowski,C.C. and Kowalczykowski,S.C. (2012) Direct imaging of RecA nucleation and growth on single molecules of SSB-coated ssDNA. *Nature*, **491**, 274–278.
28. Amitani,I., Liu,B., Dombrowski,C.C., Baskin,R.J. and Kowalczykowski,S.C. (2010) Watching individual proteins acting on single molecules of DNA. *Methods Enzymol.*, **472**, 261–291.
29. Forget,A.L. and Kowalczykowski,S.C. (2012) Single-molecule imaging of DNA pairing by RecA reveals a 3-dimensional homology search. *Nature*, **482**, 423–427.
30. Olofsson,L. and Margeat,E. (2013) Pulsed interleaved excitation fluorescence spectroscopy with a supercontinuum source. *Opt. Express*, **21**, 3370–3378.
31. Scheres,S.H. (2012) RELION: implementation of a Bayesian approach to cryo-EM structure determination. *J. Struct. Biol.*, **180**, 519–530.
32. Zheng,S.Q., Palovcak,E., Armache,J.-P., Verba,K.A., Cheng,Y. and Agard,D.A. (2017) MotionCor2 - anisotropic correction of beam-induced motion for improved cryo-electron microscopy. *Nat Methods*, **14**, 331–332.
33. Rohou,A. and Grigorieff,N. (2015) CTFFIND4: fast and accurate defocus estimation from electron micrographs. *J. Struct. Biol.*, **192**, 216–221.
34. Afonine,P.V., Poon,B.K., Read,R.J., Sobolev,O.V., Terwilliger,T.C., Urzhumtsev,A. and Adams,P.D. (2018) Real-space refinement in PHENIX for cryo-EM and crystallography. *Acta Cryst. D*, **74**, 531–544.
35. Schwede,T., Kopp,J., Guex,N. and Peitsch,M.C. (2003) SWISS-MODEL: an automated protein homology-modeling server. *Nucleic Acids Res.*, **31**, 3381–3385.
36. Pettersen,E.F., Goddard,T.D., Huang,C.C., Couch,G.S., Greenblatt,D.M., Meng,E.C. and Ferrin,T.E. (2004) UCSF chimera? A visualization system for exploratory research and analysis. *J. Comput. Chem.*, **25**, 1605–1612.
37. Adams,P.D., Afonine,P.V., Bunkóczi,G., Chen,V.B., Davis,I.W., Echols,N., Headd,J.J., Hung,L.-W., Kapral,G.J., Grosse-Kunstleve,R.W. et al. (2010) PHENIX: a comprehensive Python-based system for macromolecular structure solution. *Acta Crystallogr. D Biol. Crystallogr.*, **66**, 213–221.
38. Kowalczykowski,S.C., Clow,J., Somani,R. and Varghese,A. (1987) Effects of the *Escherichia coli* SSB protein on the binding of *Escherichia coli* RecA protein to single-stranded DNA. Demonstration of competitive binding and the lack of a specific protein-protein interaction. *J. Mol. Biol.*, **193**, 81–95.
39. Steffen,S.E., Katz,F.S. and Bryant,F.R. (2002) Complete inhibition of *Streptococcus pneumoniae* RecA protein-catalyzed ATP hydrolysis by single-stranded DNA-binding protein (SSB protein): implications for the mechanism of SSB protein-stimulated DNA strand exchange. *J. Biol. Chem.*, **277**, 14493–500.
40. Grove,D.E., Anne,G., Hedayati,M.A. and Bryant,F.R. (2012) Stimulation of the *Streptococcus pneumoniae* RecA protein-promoted three-strand exchange reaction by the competence-specific SsbB protein. *Biochem. Biophys. Res. Commun.*, **424**, 40–44.
41. Emsley,P., Lohkamp,B., Scott,W.G. and Cowtan,K. (2010) Features and development of Coot. *Acta Crystallogr. D Biol. Crystallogr.*, **66**, 486–501.
42. Morrical,S.W. (2015) DNA-pairing and annealing processes in homologous recombination and homology-directed repair. *Cold Spring Harb. Perspect. Biol.*, **7**, a016444.
43. Nayak,S. and Bryant,F.R. (2015) Kinetics of the ATP and dATP-mediated formation of a functionally-active RecA-ssDNA complex. *Biochem. Biophys. Res. Commun.*, **463**, 1257–1261.
44. Bell,J.C. and Kowalczykowski,S.C. (2016) RecA: regulation and mechanism of a molecular search engine. *Trends Biochem. Sci.*, **41**, 491–507.
45. Steffen,S.E. and Bryant,F.R. (1999) Reevaluation of the nucleotide cofactor specificity of the RecA protein from *Bacillus subtilis*. *J. Biol. Chem.*, **274**, 25990–25994.
46. Kim,T., Chitteni-Pattu,S., Cox,B.L., Wood,E.A., Sandler,S.J. and Cox,M.M. (2015) Directed evolution of RecA variants with enhanced capacity for conjugational recombination. *PLoS Genet.*, **11**, e1005278.
47. Roy,R., Kozlov,A.G., Lohman,T.M. and Ha,T. (2009) SSB protein diffusion on single-stranded DNA stimulates RecA filament formation. *Nature*, **461**, 1092–1097.
48. Gruenig,M.C., Stohl,E.A., Chitteni-Pattu,S., Seifert,H.S. and Cox,M.M. (2010) Less is more: *Neisseria gonorrhoeae* RecX protein stimulates recombination by inhibiting RecA. *J. Biol. Chem.*, **285**, 37188–37197.